

Article

On the Thermal Environmental Quality of Typical Urban Settlement Configurations

Hamed Reza Heshmat Mohajer ^{1,*}, Lan Ding ¹, Dionysia Kolokotsa ² and Mattheos Santamouris ¹¹ School of Built Environment, University of New South Wales (UNSW), Sydney, NSW 2052, Australia² Chemical and Environmental Engineering School, Technical University of Crete Kounoupidiana, GR 73100 Chania, Crete, Greece

* Correspondence: h.heshmatmohajer@unsw.edu.au

Abstract: Urban overheating and energy imbalances are severe environmental concerns. The role of urban sprawl patterns in the formation of Heat Island has recently absorbed the researchers' interest. The research focuses on metropolitan areas with a range of urban typologies. However, there still is a knowledge gap in how UHI responds to different urban typologies. The interaction between urban configurations and heat island characteristics is explored in Sydney. A combination of terrestrial surveys and modelling techniques was implemented, and results were extracted based on simulation results. The Urban Taskforce Australia suggested the applied categorization methods that follow Stewart and Oke's Local Climate Zones (LCZs) scheme. We assessed eleven urban designs on ambient air temperature, wind characteristics, heat intensity, and outdoor thermal comfort over three summer days. We correlated results to density and the built-up ratio in all configurations and found that the maximum configurational impact on the heat island reached 2.33 °C. Configurations with a built-up ratio between 0.37 to 0.5 present a sharp downward trend in the average wind speed value and indicate a minimum with a built-up ratio of 0.63. Wind maps present an increase in layouts with built-up ratios of 0.23 to 0.37, whereas they decreased with built-up ratios of higher than 0.43. The average temperature decrease in high-rise compact configurations was 1.12 °C per hour. This record is substantially higher than its open counterparts. The study showed the importance of urban configuration on thermal environmental quality. In addition, implementing appropriate urban design parameters is vital to mitigate heat islands and improve environmental thermal comfort in urban areas.



Citation: Heshmat Mohajer, H.R.; Ding, L.; Kolokotsa, D.; Santamouris, M. On the Thermal Environmental Quality of Typical Urban Settlement Configurations. *Buildings* **2023**, *13*, 76. <https://doi.org/10.3390/buildings13010076>

Academic Editor: Francesco Nocera

Received: 22 October 2022

Revised: 16 November 2022

Accepted: 18 November 2022

Published: 28 December 2022



Copyright: © 2022 by the authors. Licensee MDPI, Basel, Switzerland. This article is an open access article distributed under the terms and conditions of the Creative Commons Attribution (CC BY) license (<https://creativecommons.org/licenses/by/4.0/>).

Keywords: urban configuration; heat island; ambient air temperature; wind speed; outdoor thermal comfort

1. Introduction

Urban Heat Island (UHI) is a phenomenon resulting in the increase in ambient temperature in dense areas of cities in comparison with rural areas. UHI is relevant in the Sydney metropolitan area, with a peak intensity of up to 6 °C [1]. UHI occurs day and night, but according to [2], the maximum intensity of heat island occurs 3–5 h after sunset. This is because cities retain heat in roads, buildings, and other structures, preventing them from cooling down. The UHI phenomenon has been documented in more than 400 cities worldwide [3]. Its impact is closely related to land cover, which controls the energy budget on the earth's surface. The surface energy budget difference between the urban and rural zone, caused by various thermal-optical surface characteristics, leads to the occurrence of the UHI phenomenon [4,5]. Studies performed in Asian and Australian cities have shown how the UHI phenomenon is significant, with intensities varying between 0.4 °C and 11 °C [1]. This situation is intensified in Australia, where there is a 0.9 °C incremental rate in the annual mean temperature. The surveyed weather data over the past ten years have revealed that the number of extremely hot days is twice that of extremely cold days [6,7].

The Australian surface temperature will increase up to 5 °C by 2050. As a result, the total H/C energy requirement in Sydney (H/C balanced temperate climate) concerning the climate change predictions would rise from 120% to 530% for an energy-efficient house [6,8,9]. The urban heat gain would take its toll on human life, causing a rise in energy consumption, human discomfort, and health exacerbation. In particular, the UHI increases the demand for peak-time electricity and the consumption of cooling energy in buildings, intensifies the concentration of various harmful pollutants, increases the ecologically harmful footprint of cities, and significantly impacts health. The manifestation of the UHI phenomenon is influenced by several factors categorized into artificial and natural factors [10]. The factors generating and defining the intensity of heat islands are summarized into two broad categories; first is the meteorological factors such as the air temperature, wind speed, and direction, level of humidity, and cloud cover, and second is the urban design parameters, such as urban configuration, the density of urban areas, percentage of built-up ratios, the aspect ratio of urban canyons, sky view factor, building construction materials [11–13]. The layout and nature of buildings and their height and orientation, street width, aspect ratio, and open spaces dimensions are all included in terms of urban configuration [12,14]. Due to the different interreflections in cavities, including street canyons and courtyards, the radiation absorption rates in various city layouts are diverse and influential in indoor and outdoor environments [15]. On the other hand, wind speed has widely been reported to have lessened the intensity of the heat island effect in urban areas [11,16]. Several studies discussed the role of urban geometry on microclimate and investigated the effect of urban geometry on microclimate [17]. Their findings show that areas with shallow open spaces and wider spacing recorded temperatures 4.7 °C higher than baseline measurements from a meteorological reference. Other research used field measurements to study how urban form may affect the microclimate in different areas in Dubai [18]. They investigated street design and its impact on urban microclimate in a semi-arid climate and found that the higher the aspect ratio, the lower the temperature [19,20]. Research investigating the relationship between thermal performance and urban morphology and linking them to climatic responses stated that the configuration of a city can assist wind circulation and affects wind velocity which in turn influences temperature variations [21,22]. This research investigated the association between urban heat island intensity and wind speed and cloud cover from a network of monitoring stations in and around the large city of Melbourne, Australia. Their main findings showed that calm winds and clear skies increase urban heat island values. In the summer, it was found that an increase in wind speed by 1 m/s causes a 0.14 °C reduction in the intensity of the heat island. It was also revealed that, by increasing the cloud cover by 1 okta, UHI decreases by about 0.12 °C [16]. Wind speed is an important parameter in urban areas that influences the health, outdoor/indoor comfort, air quality, and energy consumption of the buildings [23]. The cooling effect of wind helps to mitigate the adverse effects of heat island on the microclimate and human thermal comfort. In tropical regions such as Singapore, a wind velocity of 1–1.5 m/s creates a cooling effect that is equivalent to a 2 °C drop in temperature [20,24]. Understanding the relationship between built forms and wind-induced airflow is important, particularly in the tropics where a cooling effect of urban winds is beneficial. Most of the studies carried out to understand the correlation between the built form and wind speed focused on the combination of field measurements and simulations [11]. The literature review shows previous research focused on the cooling potential of meteorological variables in urban areas. They rarely concentrated on the interaction between urban configuration and heat island effects. The main urban area parameters are layouts' density, buildings' height, and street aspect ratios. Our understanding of the interaction between ambient temperature, wind characteristics, and outdoor thermal comfort on urban parameters is limited [25]. The research was conducted under a systematic approach in Sydney climate conditions. This research aimed to bridge the gap found in the literature. We categorize layouts based on configurational characteristics into eleven typologies. A mixture of terrestrial surveys and software simulations was conducted over three summer days. The urban configuration impact on the heat island

effect was discovered by analyzing and comparing results. The results draw guidelines for implementing proper urban configurations to achieve better outdoor thermal comfort in urban areas. The report is divided into five sections. Sections 2 and 3 concentrate on the research method and applied software validation and simulation methods based on fieldwork measurements. In Section 4, we addressed how the built-up ratio and wind speed relate to the influence of urban design on heat island formation, and in Section 5, we presented our findings.

2. Materials and Methods

2.1. Field Measurement

Greater Sydney, NSW, Australia, serves as the research area's environment. Sydney, which borders the Tasman Sea to the east, is situated at 33.8° S latitude on Australia's south-east coast. With a total size of 12,367.7 km², it is the largest city in Australia. It is divided into 43 local councils, which have more than 900 state suburbs. The region runs along the coast from Gosford in the north to the Royal National Park in the south. The Blue Mountains to the west and Parr State Conservation Area are part of the area. The Sydney metropolitan region is in the Cumberland Basin, which is flat and to the south and west of Port Jackson. To the north and west, steep escarpments reach altitudes of up to 300 and 600 m above sea level, respectively, and are bordered by the Hornsby and Blue Mountains Plateaus. The Sydney urban area, as measured by the Australian Statistical Geography Standard [26], stretches 70 km from the shore in the east to the Blue Mountains in the west. Greater Sydney, which had a population of 4.92 million in June 2015, is the most populated metropolis in Australia. The city includes the eastern city and central city, and the western city is the state capital of New South Wales with UHI effects, which may peak at up to 6 °C [1]. The weather of Sydney, Australia's easternmost state, is humid subtropical (Köppen: Cfa) [27] and is characterized by warm summers and cool winters. The mean daily maximum and minimum temperatures vary between 25.9 °C in the summer (January) and 8.1 °C in the winter (July). According to historical climatic data, there are more than 30 °C days on average every 14.9 days of the year. The warmest month is January, which has an average daily air temperature range of 18.7 to 25.9 °C with a maximum temperature of 45.8 °C.

The city's distinctive urban features make the city ideal for conducting this research. The open and compact arrangement as formally defined by the Australian Association of Planners is well represented. An urban zone extending about 250 m south-north and 500 m in the east-west direction within the neighborhood of Bondi Junction, Sydney (33°53'035.400 S 151°14'058.900 E) was selected as a reference for the validation of the software. The suburbs contribute residential functions and contain a shopping and transport hub, shopping mall, casual fashion stores, and branches of some of the city's trendiest restaurants. We performed monitoring campaigns in Council St. to obtain significant results for urban climate mapping and validation of microscale models. We conducted two monitoring campaigns in Council St. during a specific day in Bondi Junction. We performed two tracks to measure the spatial and temporal distribution of the air temperature and map surface temperature within Council St. and its close surroundings. We collected microclimate data for Council St. using multiple measurement techniques on a terrestrial survey at different locations on the pedestrian level. Variables include ambient air temperature, relative humidity, wind speed/direction, incoming solar radiation, and surface temperature. Figure 1 presents a sample of the geographic coordination of the locations with their corresponding measured parameters and a summary of fieldwork measurements and recorded variables. We performed the campaign from 10:30 a.m. to 6:30 p.m. (local solar time) in Council St. on 24 October 2019, and the surrounding area.

We collected measurements at least three times at similar locations at different times to ensure redundancy.



Figure 1. The Greater Sydney area: A metropolis of three cities (**top left** figure), the Council St selected for the terrestrial campaign (**right** figure), 3D aerial view from Syd Einfeld Dr highway (**bottom left**), pictorial survey at the intersection of oxford street and Bondi Rd (**bottom right**).

2.2. Instruments and Measurement Techniques

We conducted the terrestrial survey with the following instruments and measurement techniques: The monitoring campaign area was the entire Council St. from Waverly St. to Allen Parade St. and its surrounding areas in Bondi Junction. We defined the exact location of the measurement points based on one preliminary inspection on-site led by my supervisors. We took spot measurements at many locations along Council St. and its surroundings. Measured variables include incoming solar radiation, air temperature, relative humidity, and wind speed. We performed this with a portable station mounted on a cart at 1.5 m moved along the designated track from 10:30 a.m. until 6.30 p.m., about three times per point presented in Table 1. We equipped carts with a set of sensors on the Met Pak Pro presented in Figure 2, Tables A1 and A2. A net radiometer (NR01 by Hukse flux) collected the incoming solar radiation by ISO 9060 s class pyranometer (Figure 2); A weather station (Met Pak Pro with an integrated Wind Sonic ultrasonic wind sensor by Gill Instruments, (Tables A1 and A2), Met Pak Pro weather station collected spot measurements of climatological variables (Table A1). A data logger (DT85 by Lontek) set the sampling rate for the weather station to 1 s and recorded over 30 s. Thermal camera T540 with FLIR and an infrared thermometer collected thermal information. The instruments collected surface temperatures of asphalt, sidewalks, and roof coverings, and thermal images of vertical surfaces (Table 1). The T540 is sensitive enough to detect temperature differences to <30 K to render low-noise results Table A2 present a summary of the applied equipment.

To fulfil the validity of simulations run by Envi-Met, we have chosen two distinctive tracks with different origins and destinations in the Bondi junction and implemented equipped field measurements at specific points (Table 1). In these tracks, all data collection methods were recorded and compared with simulation results which will be discussed in the next part. The pictorial study has been assessed in different situations ranging

from noon time to afternoon time and the variables including wind direction, wind speed, surface temperature, and ambient temperature have all been recorded using data equipment (Table 2). This is a powerful tool to show the credibility of this paper and proves the simulation results. As mentioned above, to validate the Envi-Met simulations we have conducted field measurements (Tables A1 and A2). All experiments were performed on sunny days and three types of pavements were classified for each path including Light concrete pavement (LCP), Dark concrete pavement (DCP), and Asphalt Road (AR).

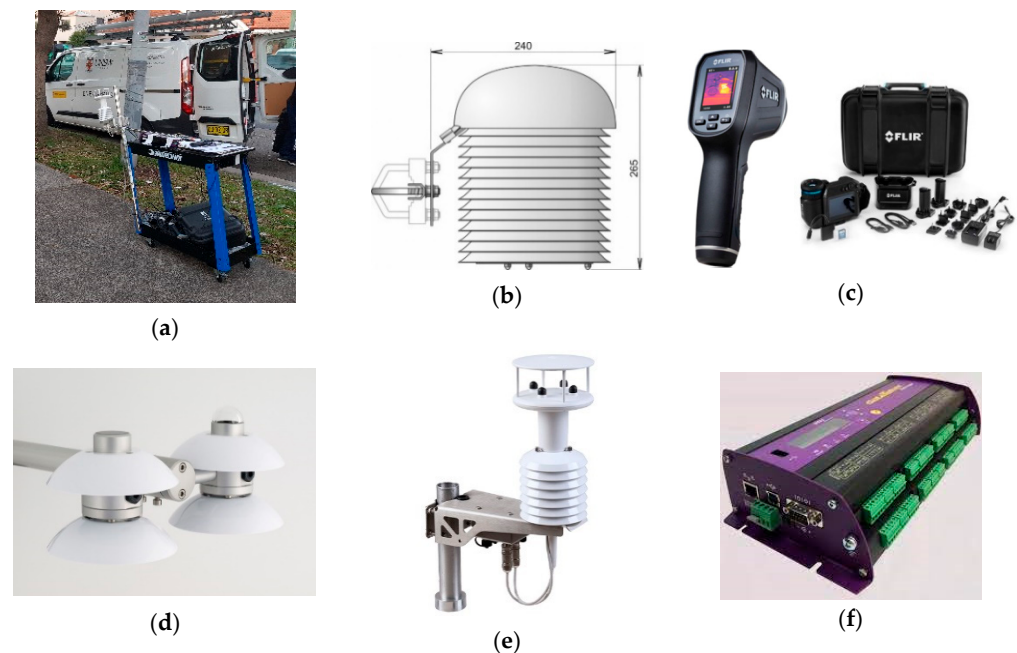


Figure 2. The MetPak Pro weather station mounted cart used for spot measurements in tracks on the left and a white radiation shield TG54 infrared thermometers integrated on the cart, respectively in the middle and on the right. (a) MetPak Pro weather station (b) White radiation shield (c) T540 by FLI and thermal gun (d) Net radiometer (e) Wind sonic ultrasonic (f) data logger (DT85 by Lontek).

We compared the real field assessments with the simulations in each track which demonstrates the range of 2.5% to 5% deviation (Figures 3 and 4). This strategy has enabled us to use and develop different building types in cities based on climatic conditions and the need for heat island mitigation as well.

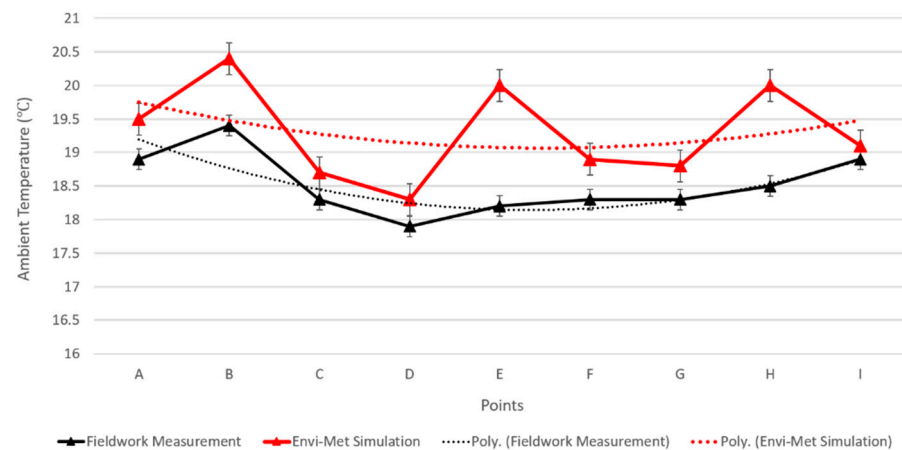


Figure 3. Comparison of ambient temperature recorded at field measurement with simulations in track 1.

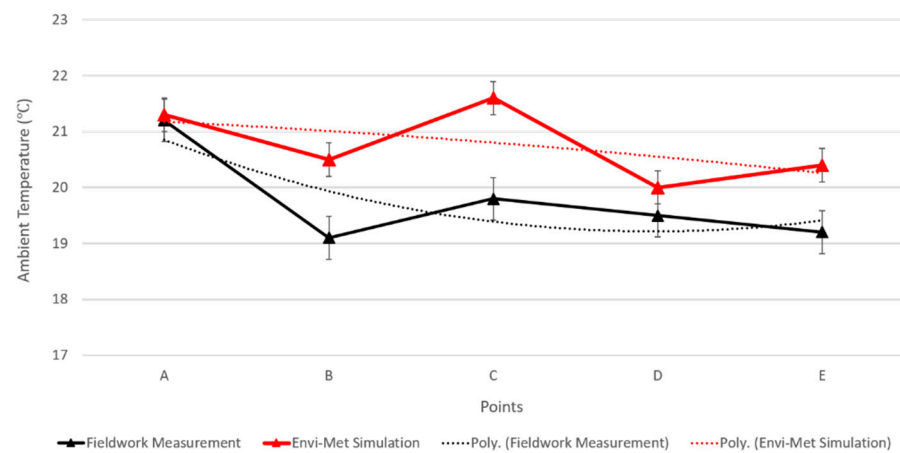


Figure 4. Comparison of ambient temperature recorded at field measurement with simulations in track 2.

2.3. Urban Classification Method

The method described below is followed to explore the correlation between urban characteristics and heat island effects.

The city of Sydney was selected as representative of humid subtropical (Köppen: Cfa) climate conditions in Eastern Australia [27]. The Sydney Metropolitan Area showcases actual neighborhoods as case studies. Being a well-established typology of open and compact designs that the Australian Association of Planners has formally described. Eleven urban areas were selected in Sydney's urban fabric as a range of urban typologies. The Urban Taskforce Australia suggested typologies following Stewart and Oke's approach in the Local Climate Zones (LCZs). We used these standardized schemes for the analysis of urban overheating conditions. The Sydney metropolitan area (SMA) profiled seven housing types for this study. The typologies defined by the Department of Planning and Environment New South Wales (NSW) on building height, density, and layout built-up ratio. It additionally distinguished the seven typologies into two types of arrangements. The letter 'O' represents an open arrangement of buildings, while the letter 'C' represents a compact arrangement of buildings. Figure 5 presents a summary of studied typologies. We classify urban areas into logical categories that can support micro-climatic analysis. Their 2D and 3D views, site dimensions, and geographical locations in Sydney are in Tables 3 and 4.

The area is characterized as a mixture of low-rise, multi-story, medium, and high-density residential, official, and commercial developments.

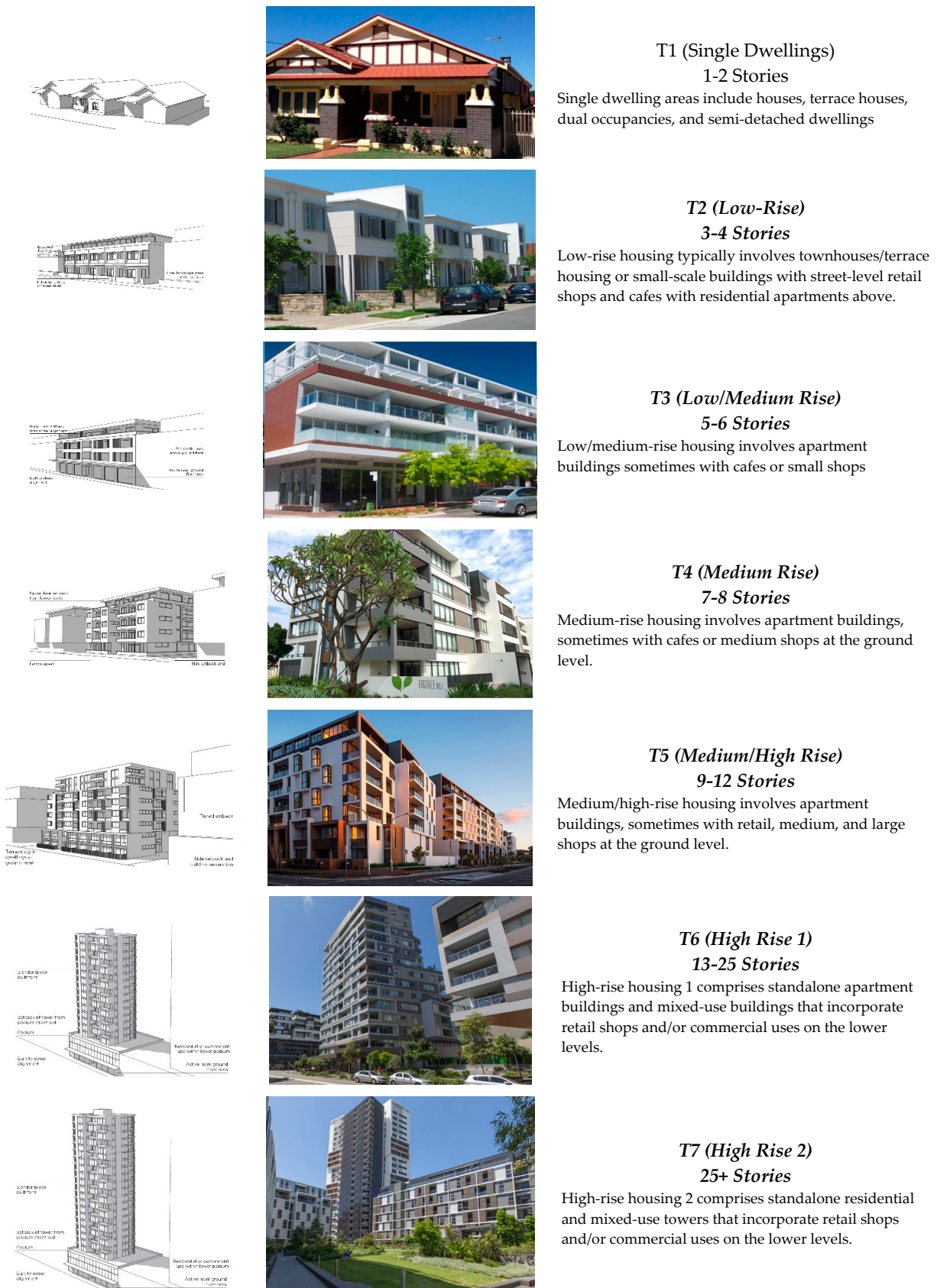


Figure 5. A summary of the housing typologies proposed based on seven building types organized in open and compact arrangements.

Table 1. Designated tracks, a sample of thermal camera picture, measured variables with their corresponding points.

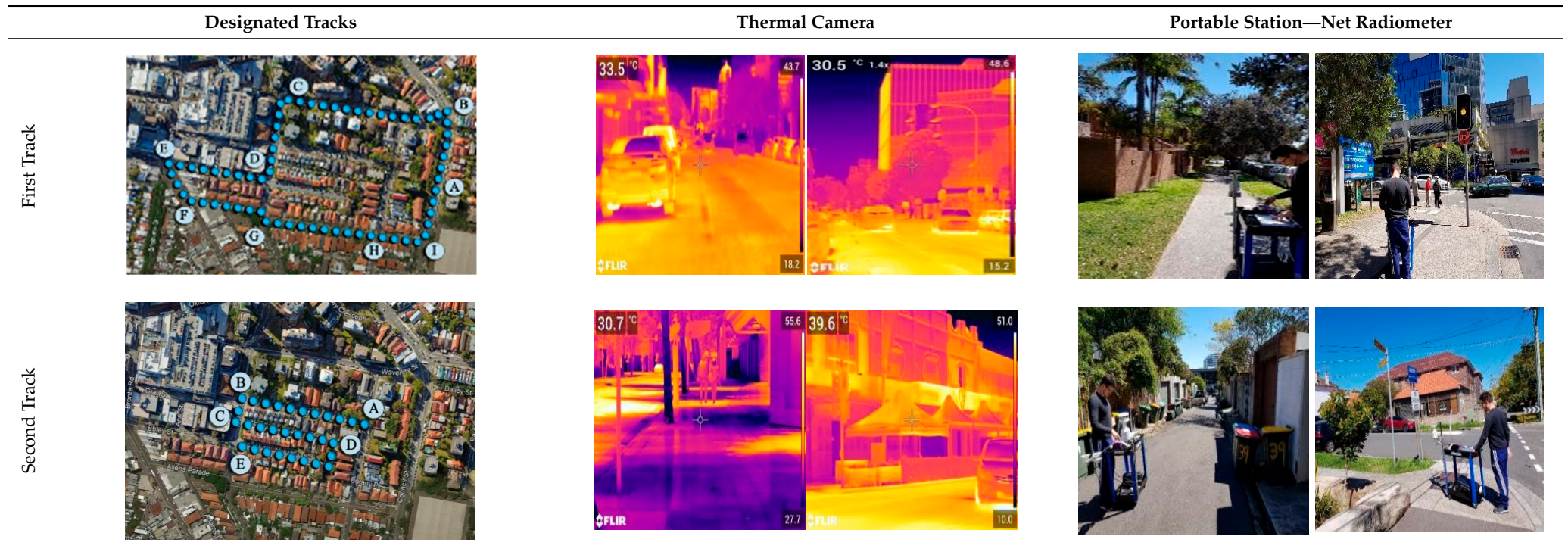


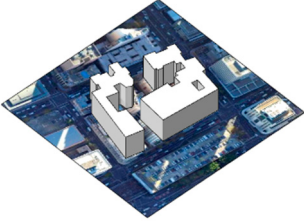
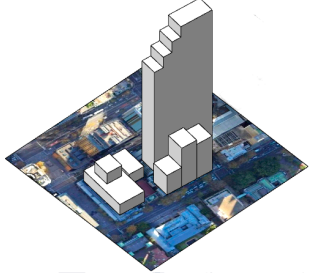
Table 2. Measured variables during the fieldwork measurements.

	A		B		C		D		E		F															
Point	-33.894004	151.254918	-33.89316	151.254928	-33.892689	151.251963	-33.894097	151.251484	-33.893156	151.25493	-33.892689	151.251963														
Record Time	10:45	11:45	16:38	16:38	11:53	10:59	12:02	11:07	12:10	11:20	12:17	10:59	13:01													
Ambient Temperature	18	18.9	17.5	17.5	19.4	18.3	19.2	17.9	19.4	18.2	19.5	18.3	19.5													
Surface Temperature	27.1	16.3	27.7	13.4	25.2	20.1	38	15	27.1	20.2	34.5	14.1	39.7	26.7	37.5	27.4	27.4	15.1	33.1	15	44	17	34.5	14	24.6	14.6
Wind Speed (m/s)	1	0.7	1.1	1.1	1.4	0.5	1.2	0.1	0.1	0.1	0.7	0.5	0.5													
Wind Direction	215	150	207	207	278	317	2	39	9	39	27	317	239													
Pavement Type	LCP		DCP		LCP		LCP		DCP		LCP															

Table 3. Open Arrangement classifications in urban configurations with their corresponding 2D, 3D view, site dimension, and locations in the city of Sydney.

Open Arrangements					
Type	OT2: Open Low Rise	OT3: Open Low/Medium Rise	OT4: Open Medium Rise	OT5: Open Medium/High Rise	OT6: Open High Rise 1
Figure					
2D Aerial View					
Google earth point	33°53'31.80" S 151°13'55.72" E	33°53'30.5" S 151°15'41.0" E	33°50'04.8" S 151°12'36.6" E	33°53'17.7" S 151°12'37.4" E	33°52'57.4" S 151°12'31.8" E
Site dimension	78.5 × 120	82.5 × 124.5	77 × 115.5	168.5 × 211	199 × 183
Address	24 Mitchell St, Centennial Park NSW 2021, Australia	Penkivil St, Bondi NSW 2026, Australia	199 Walker St, North Sydney NSW 2060, Australia	Methadone clinics, Lee St and, Little Regent St, Chippendale NSW 2008	Surry Hills NSW 2010, Australia

Table 4. Compact Arrangement classifications in urban configurations with their corresponding 2D, and 3D views, site dimensions, and locations in the city of Sydney.

Compact Arrangements					
Type	CT2: Open Low Rise	CT4: Open Medium Rise	CT5: Open Medium/High Rise	CT6: Open High Rise 1	CT7: Open High Rise 2
Figure					
2D Aerial View					
Google earth point	33°53′32.58″ S 151°14′40.03″ E	33°53′26.72″ S 151°15′43.19″ E	33°52′42.8″ S 151°12′45.2″ E	33°52′43.86″ S 151°12′28.31″ E	33°52′1.44″ S 151°12′40.65″ E
Site dimension	72 × 105	117 × 167	84 × 111	131 × 176	156 × 143
Address	47 Denison St, Bondi Junction NSW 2022, Australia	c7/99 Jones St, Ultimo NSW 2007, Australia	162–166 Goulburn St, Surry Hills NSW 2010, Australia	311–315 Castlereagh St, Haymarket NSW 2000, Australia	126–146 Phillip St, Sydney NSW 2000, Australia

3. Modelling Method

ENVI-met has been used and tested extensively for many purposes, including the impact of various urban design alternatives on the outdoor thermal environment [25,28,29]. ENVI-met-V4.4.2 is a three-dimensional microclimate model that resolves the Reynolds-averaged non-hydrostatic Navier–Stokes (RANS) equations for every spatial grid and time step [30,31]. This software is a realistic tool for modelling the distribution of the key climatic factors in metropolitan settings applied three-dimensional Computational Fluid Dynamics (CFD) model [32,33]. The software simulates surface, plant, and air interactions in an urban environment. This computer program calculates the distribution of the main climatic parameters in the urban environment. The standard version of the ENVI-met version 4.4.2 provides $250 \times 250 \times 30$ (x-y-z) cells for the simulation. It allows microscale analysis with the following features:

- Typically, the horizontal resolution is between 0.5 and 5 m;
- Typically, the time frame is between 24 and 48 h;
- Typically, the time step is between 1 and 5 s.

3.1. Resolution Settings

The area spatial resolution is rendered with the following sizes: $dx = 2$ m, $dy = 2$ m, and $dz = 1$ m. The grid at the Z-axis is telescopic and ranges from 5 to 15 in low rise to high rise, respectively. Thicker cells are set near the ground providing better accuracy. This resolution allows us to analyze small-scale interactions between individual buildings and surfaces. The research studied different settlement configuration effects on diurnal-nocturnal heat islands. We implemented the same config file, buildings' materials, soil, and surface in all classifications while ignoring urban greenery. The classifications rotate degrees out of the north axis to mimic geographical properties.

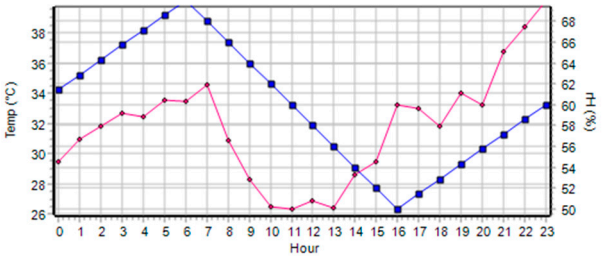
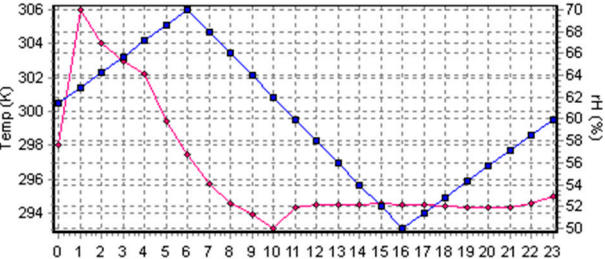
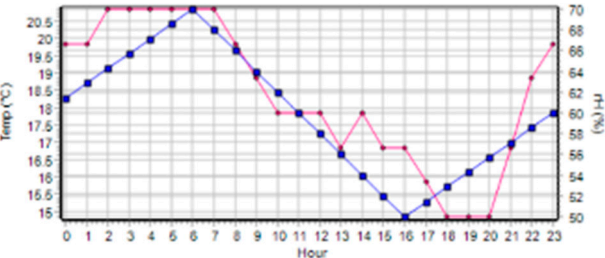
3.2. Simple Forcing

Three summer day representatives of the ideal hot summer day were chosen for conducting this research. We derived ambient air temperature data from a fixed weather station installed in the Bondi Junction precinct. As the spatial distribution of the simulated models is within a close distance to Bondi or based in a similar urban context, we collected this station as the reference. The climatological data profiles are applied as a reference point for comparing results. As the wind pattern is influenced by the urban surface in the boundary layer significantly across the Bondi area, we collected its' record from BOM. We took the initial wind speed and direction from the Bureau of Meteorology (Observatory Hills weather station). Observatory Hill ($151^{\circ}12'18''$ E) is on a hill covered by greenery. It is close to the coast and Sydney's central business district (CBD), extending over 27 km², with a tree canopy cover of approximately 15.2%. The wind mostly blows from the sea to the site, and NE/SE winds represent the sea breeze. NW/SW winds blow from inner Sydney towards the reference station. To provide a holistic understanding of the correlation between urban configuration and the HI effect, we collected three ideal days corresponding to the heat wave period in Sydney for this study. The climatological variables differ regarding wind speed/direction and ambient air temperature. The relative humidity forced a linear profile to reflect its' logical trend under studied climate conditions on an hourly basis. In addition, its impact on the heat island is not in the scope of this research and remained the same for all three days. We calculated ambient air temperature and relative humidity at 2 m and wind speed at 10 m above the ground. Table 5 presents the main meteorological variables applied in the simulation domain.

A summary of simulations presented under the following different days in Table 5: 1–17 January: High ambient air temp, low wind speed, wind direction = east/2–24 January: Moderate ambient air temp, moderate wind speed, wind direction = north/3–19 February: Low ambient air temp, high wind speed, wind = south-east. We applied simple forcing simulation methods for ambient air temperature and wind speed/direction. We performed the simulations for 24 consecutive hours, starting from 1 a.m. to 24 p.m. at the human

height level (H = 1.6 m) on these three days in all typologies. We have considered the 24 h cycle to balance computational time and precision of the outputs. Results from 6 a.m. to 6 p.m. reflect a diurnal heat island; the rest are nocturnal.

Table 5. Meteorological condition of three summer day (A = Wind speed measured in 10 m height (m/s), B = Wind direction(0 = North and 180 = South, C = Relative humidity in 2 m (%), D = Roughness length at measured site, E = Specific humidity at model top and F = Minumum/maximum temperature (°C)).

Thermal and Humidity Profile	A	B	C	D	E	F
 <p>17 January</p>	2	90	50	0.01	7	26.35–40.17
 <p>24 January</p>	5	0	50	0.011	7	19.95–38.27
 <p>19 February</p>	7.5	135	50	0.01	7	14.85–20.85

A comparison of the input ambient air temperature into the Envi-met software is presented in Figure 6.

3.3. Comfort Evaluation

We calculated comfort indices using ENVI-met Biomet that applied calculated human comfort which is called the “Predicted Mean Vote”, or PMV [33]. The PMV is a thermal comfort index based on empirical relationships between the metabolic rate of activity and the body’s mean skin temperature and evaporative heat loss under comfort conditions. We assumed a typical male (35 years old; 1.75 tall; weight 75) for the thermo-physiological parameters of the human body. The person wears clothing values of 0.5 (corresponding to summer business suits) and an activity level of 1.4 MET. We studied layouts on main climatological variables. These include (maximum/minimum ambient air temperature, wind speed, wind direction, and heat intensity).

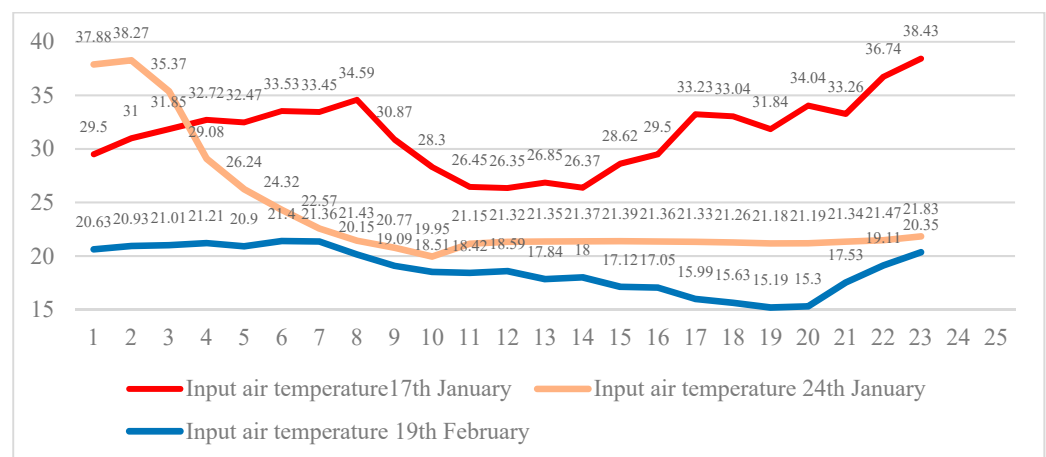


Figure 6. Input air temperature comparison in three summer ideal day.

4. Simulation Results

This section presents the effect of eleven configurations on heat island characteristics under three ideal summer days, summarized in Table 6. The results are studied, discussed, and presented in a comparative format. UHII differs from the Bondi Junction fixed weather station as the reference. The UHII of a single station at a specific hour is the difference between the dry-bulb temperature of the station and that of the reference station and the daily UHII is defined as the average value of the hourly UHII.

$$\text{UHII} = T_{\text{station}} - \text{Preference}$$

Table 6. Summary of input ambient air temperature data to Envi-met software derived from the fixed weather station in Bondi precinct.

	1	2	3	4	5	6	7	8	9	10	11	12
17 January	29.5	31	31.85	32.72	32.47	33.53	33.45	34.59	30.87	28.3	26.45	26.35
24 January	37.88	38.27	35.37	29.08	26.24	24.32	22.57	21.43	20.77	19.95	21.15	21.32
19 February	20.63	20.93	21.01	21.21	20.9	21.4	21.36	20.15	19.09	18.51	18.42	18.59
	13	14	15	16	17	18	19	20	21	22	23	
17 January	26.85	26.37	28.62	29.5	33.23	33.04	31.84	34.04	33.26	36.74	38.43	
24 January	21.35	21.37	21.39	21.36	21.33	21.26	21.18	21.19	21.34	21.47	21.83	
19 February	17.84	18	17.12	17.05	15.99	15.63	15.19	15.3	17.53	19.11	20.35	

Configuration is evaluated based on the main climatological variables' maximum, minimum, and average values. These include ambient air temperature, wind speed/direction, heat island intensity, and prediction of hourly temperature decrease along their canyons. The heat map presents the distribution of the ambient air temperatures with their corresponding wind map rendered at the diurnal and nocturnal periods at 1.6 m height above ground level.

We calculate the built-up ratio of the individual precinct. In this case, the floor area ratio (FAR) is the measurement of a building's floor area to the size of the lot/parcel in which the building is located. FAR is expressed as a decimal number and is derived by dividing the total area of the building by the total area of the parcel (building area ÷ lot area). We applied 3D Google street view to generate the 2D map of each precinct. A precise boundary of the selected map cropped that can be applied as a reference for the total precinct area. AutoCAD software was applied to draw the boundary lines of buildings to calculate the gross built-up of the selected precinct. Then we correlate the result to the built-up ratio of the selected precincts to extract the possible interactions.

We have considered the 24 h cycle to balance computational time and precision of the outputs. Results from 6 a.m. to 6 p.m. reflect a diurnal heat island and the rest are considered nocturnal.

4.1. Compact Arrangements and Heat Island Effect

A study of heat maps indicates that 4 p.m., 1 p.m., and 7 a.m. present the maximum diurnal ambient air temperature on 17, 24 January, and 19 February, respectively. Nocturnal maximum value present at 11 p.m., 1 am, and 5 a.m. on 17, 24 January, and 19 February, respectively. Tables A3 and A4 in Appendix A present a summary of the heat map simulated employing Envi-met. Diurnal maximum ambient air temperature ranged from 38.99 °C in CT4 on a north-south oriented canyon with poor ventilation on 17 January to 20.17 °C in the middle of a north-south oriented canyon in the middle of the buildings in CT4. All the settlements present higher diurnal heat intensity than nocturnal with a maximum of 6.01 °C on 17 January in CT2. The wind speed varies from 1.28 m/s in CT2 in a blocked canyon to 12.55 m/s in CT7 near the building's edges. Generally, arrangements include urban canyons with higher aspect ratios, and high-rise buildings present higher wind speed, larger shading areas, and improve outdoor thermal comfort. Table 7 presents a summary of the main climatological variables during three typical summer days periods in compact arrangements.

Table 7. Summary of the main climatological variables extracted from the heat map in all compact arrangements.

Precinct	Simulation Period	T		Wind Speed	Max Heat Intensity		Temperature Decrease		Canyon Properties		Ventilation
		Max	Min		Diurnal	Nocturnal	Total	Average	Aspect Ratio	Orientation	
CT2	17 January	34.67 °C	28.17 °C	1.28 m/s	6.01 °C	1.71 °C	36.74 °C	1.530 °C	0.45	N-S	Blocked
	24 January	23.54 °C	20.70 °C	4.05 m/s	2.33 °C	0.35 °C	19.88 °C	0.828 °C	0.41	E-W	Moderate
	19 February	20.51 °C	14.68 °C	5.59 m/s	2.01 °C	0.53 °C	17.5 °C	0.729 °C	0.43	N-S	Uniform
CT3	17 January	38.96 °C	27.3 °C	3.082 m/s	4.23 °C	1.44 °C	32.36 °C	1.348 °C	0.79	N-S	Uniform
	24 January	28.91 °C	20.5 °C	4.63 m/s	2.05 °C	0.45 °C	23.05 °C	0.96 °C	0.54	E-W	Moderate
	19 February	20.17 °C	14.55 °C	6.65 m/s	1.1 °C	0.41 °C	15.71 °C	0.654 °C	0.43	N-S	large masking
CT4	17 January	38.99 °C	27.4 °C	3.89 m/s	4.73 °C	2.74 °C	37.73 °C	1.572 °C	1.062	N-S	blocked
	24 January	29.64 °C	20.52 °C	5.74 m/s	2.01 °C	0.64 °C	24.24 °C	1.01 °C	0.64	N-S	masking area
	19 February	20.26 °C	14.75 °C	9.19 m/s	1.16 °C	1.42 °C	18.78 °C	0.782 °C	1.1	N-S	moderate
CT5	17 January	38.96 °C	27.3 °C	3.082 m/s	4.73 °C	2.74 °C	48.89 °C	2.037 °C	3.1	E-W	Blocked
	24 January	29.75 °C	20.86 °C	4.23 m/s	2.52 °C	0.63 °C	24.96 °C	1.04 °C	3.1	E-W	Masking area
	19 February	20.17 °C	14.55 °C	9.15 m/s	1.38 °C	1.01 °C	19.11 °C	0.796 °C	2.4	N-S	Blocked
CT6	17 January	39.18 °C	27.6 °C	5.5 m/s	4.16 °C	2.23 °C	33.56 °C	1.393 °C	7.5	N-S	uniform
	24 January	20.8 °C	29.75 °C	6.07 m/s	2.01 °C	0.64 °C	20.34 °C	0.847 °C	4.76	E-W	blocked
	19 February	20.3 °C	15.3 °C	12.47 m/s	1.41 °C	1.21 °C	19.01 °C	0.792 °C	3–5.2	N-S	uniform
CT7	17 January	38.72 °C	27.4 °C	5.5 m/s	4.16 °C	2.23 °C	36.14 °C	1.505 °C	4.32	N-S	moderate
	24 January	29.75 °C	20.6 °C	6.02 m/s	2.01 °C	0.64 °C	21.56 °C	0.898 °C	4.2–4.32	E-W	blocked
	19 February	20.23 °C	14.63 °C	12.55 m/s	1.1 °C	1.39 °C	26.16 °C	1.09 °C	4.2–4.32	E-W	moderate

There is a high difference in maximum ambient air temperature between compact arrangements from 7 a.m. to 6 p.m. In addition, it can be deduced that ambient air temperature increases more rapidly in low-rise arrangements (e.g. CT2 dotted in orange) compare to the high-rise (e.g., CT7 dotted in dark blue) buildings in the nocturnal period. The regression function formula derived from the power equation of data predicted the increase of ambient air temperature in individual settlements during this 24-h cycle as outlined in Figure 7. CT2 with an equation of $y = 29.976x^{0.04}$ predicted the maximum increase while CT7 with an equation of $y = 30.536x^{0.0255}$ predicted the minimum increase

during the simulated period. It can be a result of lower wind speed, poor adjacent building shading, and low canyons aspect ratio that highly influences the heat flow in an urban environment. On the other hand, low-rise arrangements predicted lower ambient air temperature during the nocturnal period. It is assumed that this is the result of a higher heat advection rate in these arrangements. CT7 and CT6 present almost similar values during the 24-h cycle. The comparison summary of the diurnal and nocturnal ambient air temperature distribution map in CT2, CT4, and CT7 on 17 January is present in Table 8.

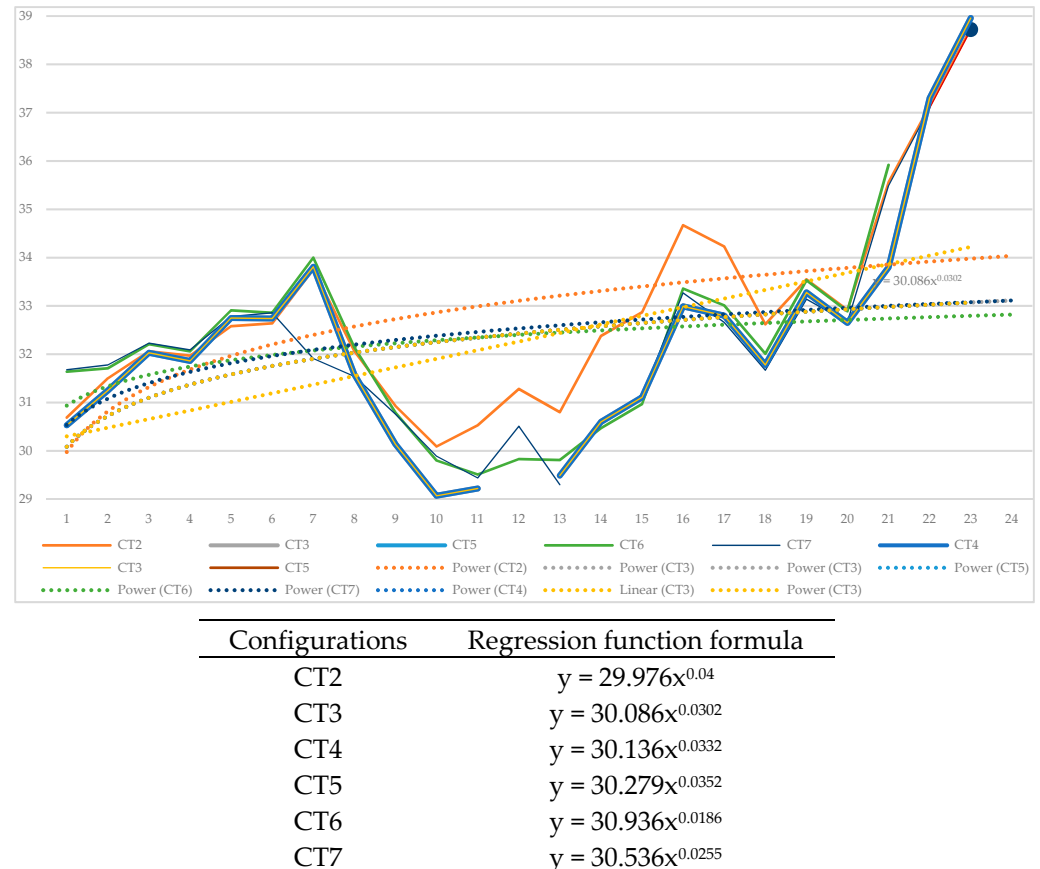


Figure 7. Maximum ambient air temperature in compact-type arrangement on 17 January with their associated regression function formula.

Layout configuration in Compact Type two comprises two north-south and one east-west orientated canyons with a connected courtyard. A summary of the distribution of diurnal- nocturnal ambient air temperatures with their corresponding wind map during three summer days is provided in Appendix A.2. On 17 January, the ambient air temperature reached a maximum of 34.67 °C in the north-south canyon, with a low wind speed, a large masking area, and an aspect ratio of 0.45. While the minimum temperature in the canyon with a similar orientation was 14.68 °C with an aspect ratio of 0.43 perpendicular to the wind flow, and the average wind speed was close to 4.30 m/s on 19 February, as described in Appendix A.2. Layout configuration compact type three comprises five narrow east-west orientated canyons and three wide north-south canyons. Ambient temperature varies between 38.96 °C in the north-south canyon; wind speed close to 3.08 m/s uniform ventilation and aspect ratio close to 0.79 on 17 January to 14.55 °C in the canyon with a similar orientation, aspect ratio = 0.43 and average wind speed close to 6.65 m/s on 19 February, as summarized in Appendix A.2. Compact type four comprises one square-shaped courtyard surrounded by high to mid-rise buildings. Three narrow east-west canyons and one north-south canyon serve as traffic roads. Ambient temperature varies between 38.99 °C in the north-south canyon, wind speed close to 3.89 m/s uniform ventilation, and aspect ratio

close to 1.062 on 17 January to 14.75 °C in the canyon with a similar orientation, aspect ratio = 1.1 and average wind speed close to 9.19 m/s in 19 February, as summarized in Appendix A.2. Compact type six comprises three connected courtyards that are surrounded by high-rise buildings. One north-south and two wide west-east canyons limit the area. The internal courtyard presents almost no circulation during these three days and remains constant, with an average value close to 1 m/s. The adjacent building's high wind shading blocked the airflow. The maximum ambient temperature is 38.96 °C in east-west canyons, wind speed close to 3.082 m/s, blocked ventilation, and aspect ratio of 3.1 on 17 January. A similar orientation canyon shows a minimum of 14.55 °C with an aspect ratio of 2.4 and an average wind speed close to 9.15 m/s on 19 February. Appendix A.2 presents a summary of the data. Compact type six comprises two narrow, one-wide connected courtyards surrounded by high-rise buildings with the north-south orientated and two wide west-east orientated canyons. The wind map presents moderate wind circulation in the internal courtyard with a high wind masking area, an average value close to 1 m/s. Adjacent buildings block natural wind flow in the courtyard. North-south canyon with a wind speed of 3.082 m/s, uniform ventilation, and aspect ratio close to 7.5 presented a maximum ambient temperature of 38.18 °C on 17 January. A canyon with a similar orientation, aspect ratio = 3–5.2, and average wind speed close to 12.47 m/s shows a minimum of 15.3 °C on 19 February. Appendix A.2 presents a summary of the data. Compact Type Seven layout comprises two narrow east-west and one-wide north-south canyons. High-rise buildings surrounded the canyons and created deep courtyards. In this layout, north-south canyons in the middle of high-rise buildings with an aspect ratio close to $(h/w) = 8.07$ present a maximum of 38.72 °C temperature on 17 January. An extensive area with an east-west canyon aspect ratio of 4.32 exposed to the east shows a minimum of 14.63 °C with an average wind speed close to 9.33 m/s on 9th February. Table 9 present a comparison summary of the wind speed/direction distribution map across compact-type arrangements on 17 January.

A detailed analysis of the wind map simulated with the initial wind speed of 2 m/s flow from the east on 17 January was performed. The wind characteristics remain almost constant along all models during the simulation period. A large proportion of the urban area presents lower wind speed values compared to the initial boundary condition with a large vortex zone in the courtyard and wind leeward area. There is a close connection between the wind direction and layout configuration. A comparison of the wind map reveals that wind direction plays an important role in a layout wind circulation rate while wind speed alteration impacts the vortex area size and higher wind speed doesn't necessarily result in better layout ventilation. CT2 presents a minimum value close to 0.32 m/s in the leeward zone, and an average of 1.39 m/s in canyons with perpendicular orientation to the wind flow to a maximum value close to 3.44 m/s in the middle of the canyon, with the east-west orientation aspect ratio = 0.73 parallel to the wind flow. CT4 presents almost high wind shading with a large area presenting a very low wind speed value. The internal courtyard presents almost no circulation during three days with an average value close to 1 m/s. CT7 presents a relatively high circulation rate along the precinct with two wide canyons and one narrow canyon parallel to the wind flow with an average in the middle close to 4.53 m/s. A summary of outdoor thermal comfort in selective compact-type arrangements is presented in Table 10.

Canyon and courtyards with high aspect ratios in high-rise arrangements predicted low PMV value as the result of building shading masks. On another hand, low aspect ratio asphalt paved canyons with large wind masking areas predicted PMV = 3.

Table 8. A comparison summary of diurnal and nocturnal ambient air temperature distribution map across compact-type arrangements on 17 February.

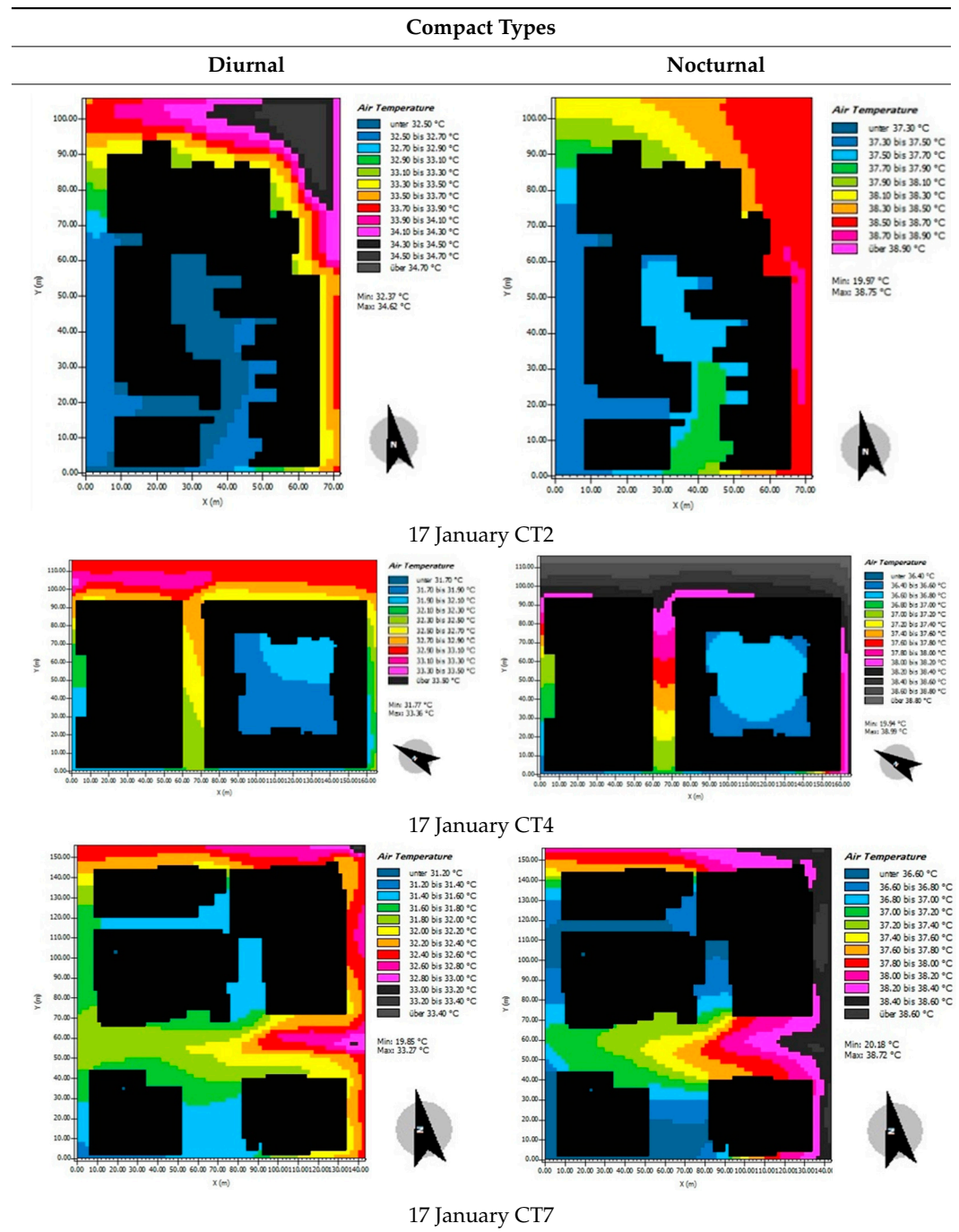


Table 9. Summary of wind speed/direction distribution map across compact-type arrangements on 17 January.

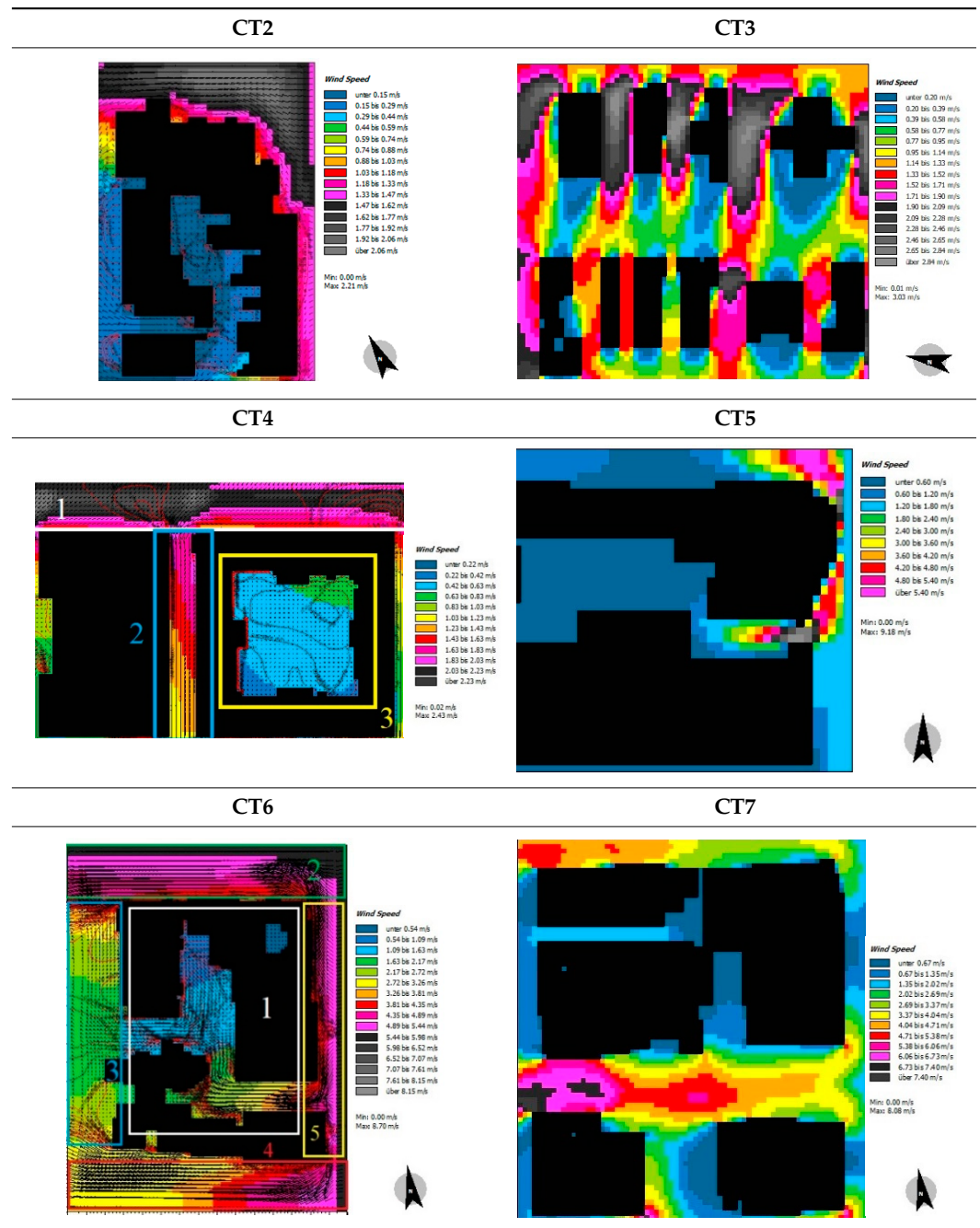
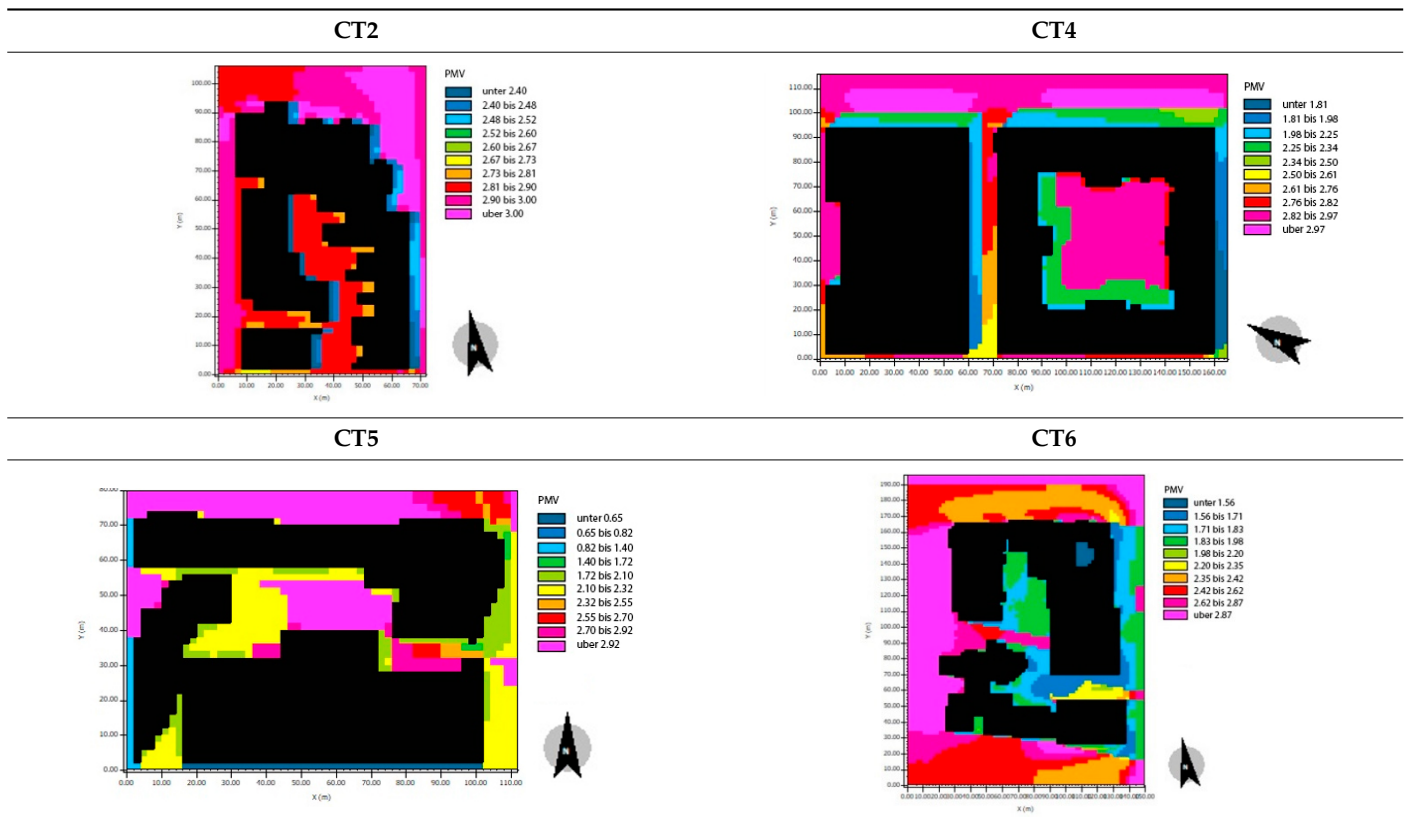


Table 10. Summary of the outdoor thermal comfort based on PMV in compact-type arrangement on 17 January.



4.2. Open Type Arrangements and Heat Island Effect

Diurnal and nocturnal heat islands are similar in the compact arrangement regarding their occurrence period. Appendix A.2 presents a summary of the heat map simulated employing Envi-met. A study of heat maps predicted the maximum diurnal heat intensity in OT2 to be 6.7 °C on 17 January. Maximum ambient air temperature ranges from 20.13 °C in OT3 on a north-south oriented canyon with blocked ventilation on 19 February and nocturnal heat islands are similar in the compact arrangement regarding their occurrence period. Appendix A.2 presents a summary of the heat map simulated employing Envi-met.

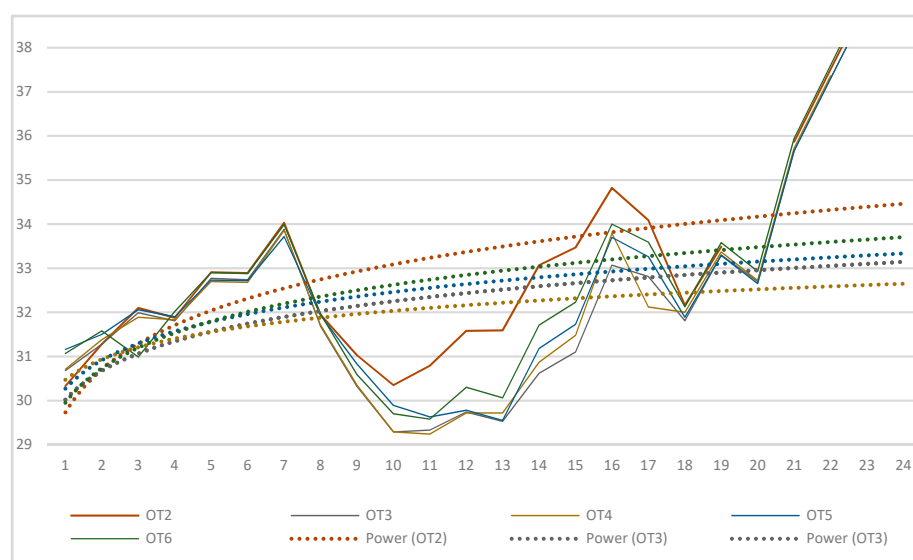
A study of heat maps predicted the maximum diurnal heat intensity in OT2 to be 6.7 °C on 17 January. Maximum ambient air temperature ranges from 20.13 °C in OT3 on a north-south oriented canyon with blocked ventilation on the 19 of February to 39.27 °C in OT6 on a north-south oriented canyon with moderate ventilation on the 17 of January. Diurnal heat intensity outweighs nocturnal in open-type arrangements. Wind speed varies from 2.07 m/s in OT5 in a blocked canyon to 6.56 m/s in a canyon aspect ratio close to 0.79, parallel to the wind speed in OT3. Generally, arrangements include urban canyons with higher aspect ratios, and high-rise buildings present higher wind speed, larger shading areas, and improve outdoor thermal comfort. Table 11 presents the main climatological variables during three ideal summer days periods in open-type arrangements.

OT6 with 29.24 °C at 11 a.m. and OT2 with 34.82 °C at 4 p.m. present the maximum ambient air temperature difference between open-type arrangements in the diurnal period. Additionally, it can be deduced that ambient air temperature increases more rapidly in low-rise arrangements (e.g., OT2 dotted in brown) compare to the high-rise (e.g., OT6 dotted in dark green) buildings. The regression function formula derived from the power equation of data predicted the increase of ambient air temperature in individual settlements during this 24-h cycle as outlined in Figure 8. OT2 with an equation of $y = 29.732x^{0.0464}$

predicted the maximum increase while OT4 with an equation of $y = 30.473x^{0.0217}$ predicted the minimum increase during the simulated period.

Table 11. Summary of main climatological variables during the simulation period in open-type arrangements.

Precinct	Simulation Period	Ambient Temperature in the Canyon			Max Heat Intensity		Temperature Decrease		Canyon Properties		Ventilation
		Max	Min	Wind Speed	Diurnal	Nocturnal	Total	Average	Aspect Ratio	Orientation	
OT2	17 January	39.14 °C	27.2 °C	2.016 m/s	6.7 °C	2.61 °C	51.31 °C	2.137 °C	0.41	E-W	uniform
	24 January	28.24 °C	19.81 °C	3.52 m/s	3.45 °C	0.43 °C	38.15 °C	1.589 °C	0.45	N-S	uniform
	19 February	20.16 °C	14.2 °C	4.37 m/s	1.1 °C	1.39 °C	14.48 °C	0.603 °C	0.45	N-S	moderate
OT3	17 January	38.96 °C	27.2 °C	2.89 m/s	4.25 °C	2.4 °C	32.67 °C	1.361 °C	0.79	N-S	uniform
	24 January	30.24 °C	20 °C	4.92 m/s	1.29 °C	2.24 °C	23.39 °C	0.974 °C	0.79	N-S	moderate
	19 February	20.13 °C	14.62 °C	6.56 m/s	1.13 °C	0.32 °C	13.22 °C	0.550 °C	0.79	N-S	blocked
OT4	17 January	38.99 °C	27.4 °C	2.22 m/s	5.09 °C	2.47 °C	37.73 °C	1.572 °C	0.12	N-S	uniform
	24 January	29.46 °C	20.94 °C	4.96 m/s	1.74 °C	0.66 °C	15.98 °C	0.665 °C	0.34	N-S	uniform
	19 February	20.16 °C	14.55 °C	5.85 m/s	1.31 °C	0.69 °C	14.06 °C	0.585 °C	0.12	N-S	moderate
OT5	17 January	38.93 °C	27.12 °C	2.07 m/s	4.81 °C	2.471 °C	37.47 °C	1.561 °C	1.02	E-W	blocked
	24 January	29.69 °C	20.58 °C	4.60 m/s	1.95 °C	0.67 °C	22.52 °C	0.938 °C	1.02	E-W	moderate
	19 February	20.22 °C	14.63 °C	6.43 m/s	1.29 °C	0.92 °C	18.37 °C	0.765 °C	1.02	E-W	blocked
OT6	17 January	39.27 °C	27.8 °C	4.39 m/s	5.34 °C	2.69 °C	33.86 °C	1.410 °C	0.98	N-S	moderate
	24 January	30.4 °C	20.88 °C	4.60 m/s	2.01 °C	0.94 °C	23.94 °C	0.997 °C	1.3	N-S	moderate
	19 February	20.41 °C	14.82 °C	6.55 m/s	1.23 °C	0.82 °C	15.98 °C	0.665 °C	1.3	N-S	blocked

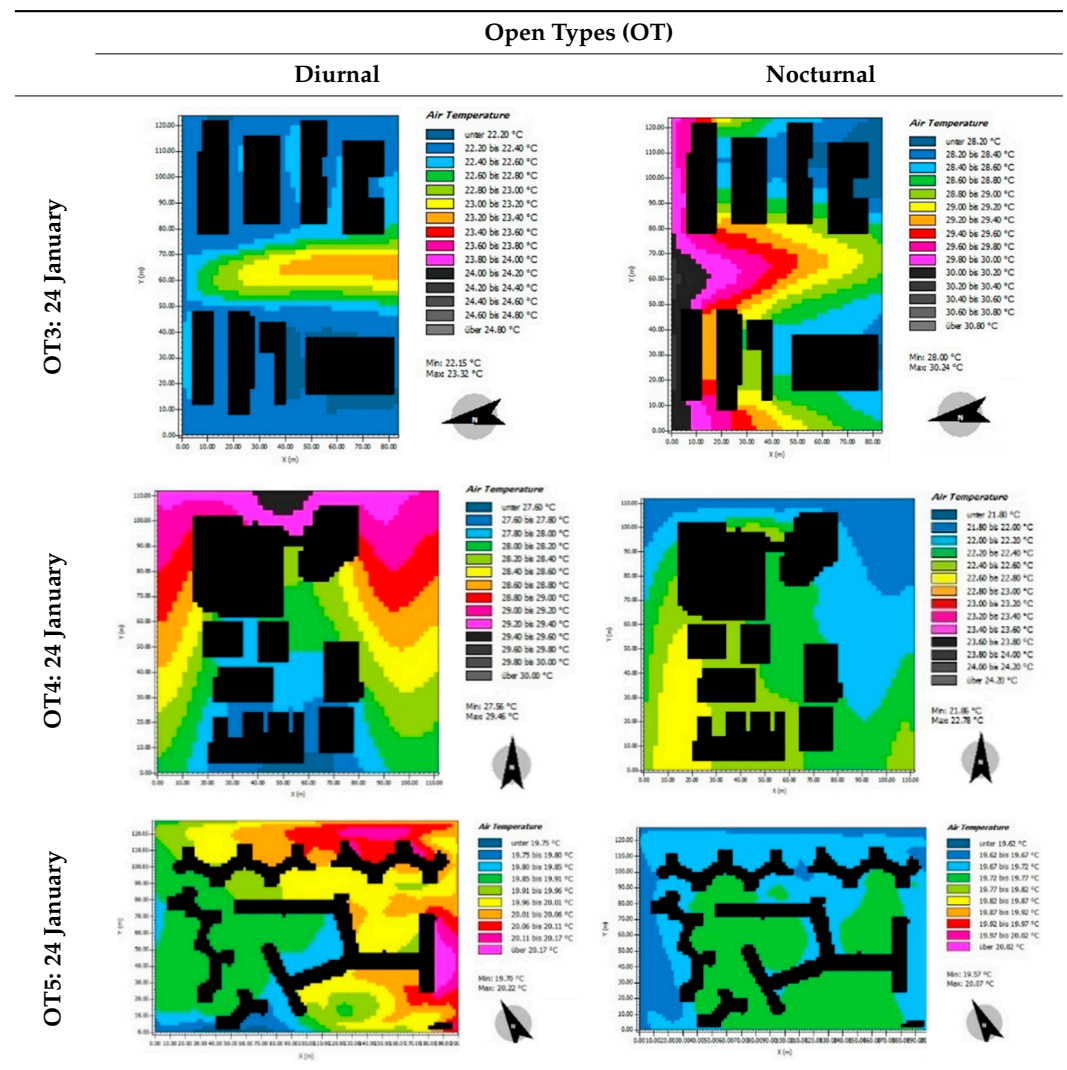


Configurations	Regression function formula
OT2	$y = 29.732x^{0.0464}$
OT3	$y = 30.019x^{0.0312}$
OT4	$y = 30.473x^{0.0217}$
OT5	$y = 30.27x^{0.0304}$
OT6	$y = 29.951x^{0.0371}$

Figure 8. Summary of the maximum ambient air temperature values derived from the analysis of the heat map on 17 January in open types arrangements with their associated regression function formula.

The comparison summary of the diurnal and nocturnal ambient air temperature distribution map in OT3, OT4, and OT5 on 24 January is present respectively in Table 12.

Table 12. Comparison summary of diurnal and nocturnal ambient air temperature distribution map in OT3, OT4, and OT5 on 24 January.



Open Type two comprises one narrow, one wide north-south, and one wide east-west canyon. Canyons with an east-west orientation, aspect ratio (h/w) = 0.416 in the middle of the layout, present a maximum temperature of 39.14 °C. In a small area near the building edge perpendicular to the wind flow, the average wind speed close to 4.37 m/s shows a minimum of 14.20 °C at 8 p.m. on 19 February. **Open type three** layout comprises two narrow and one-wide north-south oriented canyons. There are five narrow east-west oriented canyons created between buildings. A north-south-oriented canyon with an aspect ratio of 0.79 shows a maximum temperature of 38.96 °C on 17 January. A narrow east-west and north-south canyons parallel to the wind flow with an average wind speed close to 4.63 m/s present a minimum ambient temperature of 14.62 °C on 19 February.

Open Type four comprises two wide north-south canyons and two narrow east-west canyons. There is an extensive highway on the east side of the layout close to the mid-rise buildings. A north-south canyon with an aspect ratio between 0.12 to 1.282 exposed to the east presents a maximum temperature of 38.99 °C. An extensive area on the east side of the layout paralleled wind flow, and an average wind speed close to 5.12 m/s in the middle of the canyon presented a minimum of 14.55 °C on 19 February. **Open Type five** comprises two north-south and two east-west canyons with extensive areas surrounded by mid-to high-rise buildings. In an east-west canyon exposed to the north, an aspect ratio close to (h/w) = 1.02 with 38.93 °C presents the maximum temperature. A large area on the east

side of the layout with an E-W orientation almost parallel to wind flow along the canyon presented a minimum of 14.75 °C on 19 February.

Open Type six comprises two north-south and two east-west orientated canyons with a large open area on the west side of the precinct. An extensive area with almost north-south orientation exposed to the west, near the wide asphalt paved traffic road and one side no building coverage aspect ratio close to $(h/w) = 0.54$ presents a maximum temperature of 39.27 °C summarized in Table 13. The minimum presented in the large area on the east side of the layout with north-south orientation almost parallel to wind flow along the canyon, with the average wind speed close to 5.08 m/s in the middle of the canyon by 14.90 °C on 19 February. The date of 17 January presents maximum diurnal and nocturnal heat intensity by 5.34 °C at 2 p.m. and 2.69 °C at 9 p.m.

We simulated models with the initial wind speed of 7.5 m/s flow from the southeast on 19 February. The diurnal heat island effect occurred at 7 a.m. while the nocturnal was predicted to be at 5 a.m. in all configurations on 19 February. In most of the case studies, urban asphalt paved roads in canyons with north-south orientation predicted higher ambient air temperature. The maximum diurnal ambient air temperature ranges from 20.41 °C in OT6 to 20.16 °C in OT2 and the nocturnal range is from 20.31 °C in OT6 to 19.94 °C in OT2. The general trend of data presents similar results compared to the compact type arrangements. OT2 with one east-west canyon parallel to the wind speed presents a maximum of 6.41 m/s in the middle of the canyon. A north-south canyon parallel to the wind flow presents a maximum of 6.56 m/s close to the building edge in the middle of the canyon on OT3. An east-west canyon parallel to the wind and two north-south canyons predict a maximum of 5.85 m/s in the middle of the canyon with a large masking area between the leeward side of the buildings in OT4. OT5 predicted an east-west canyon parallel to the wind with a maximum of 6.43 m/s in the middle of the canyon and near the building edge with the largest masking area between the leeward side. PMV. Table 14 present a summary of outdoor thermal comfort based on the PMV indices in open arrangements on 19 February. All configurations present uncomfortable (warm to hot, PMV close to 3) outdoor thermal conditions in the middle of asphalt-paved canyons. Canyons with low aspect ratio, not enough solar protection by the adjacent building, and poor ventilation rate predicted higher PMV. OT2 reveals that higher PMV value is frequent in east-west orientated canyons', aspect ratio $(h/w) = 0.416$. Canyons with an east-west orientation, aspect ratio $(h/w) = 0.79$ in the middle of the layout present higher PMV values in OT3 in narrow canyons influenced by the adjacent building shade predicted of low PMV value. In OT4 there is a frequency of higher PMV in a north-south oriented canyon exposed to the east, the aspect ratio varies between $(h/w) = 0.12$ to 1.282 in the middle of the layout. Canyons with east-west orientation expose to north, aspect ratio close to $(h/w) = 0.2$ in OT5 predicted higher PMV value.

Table 13. A comparison summary of wind speed/direction distribution map across open-type arrangements on 19 February.

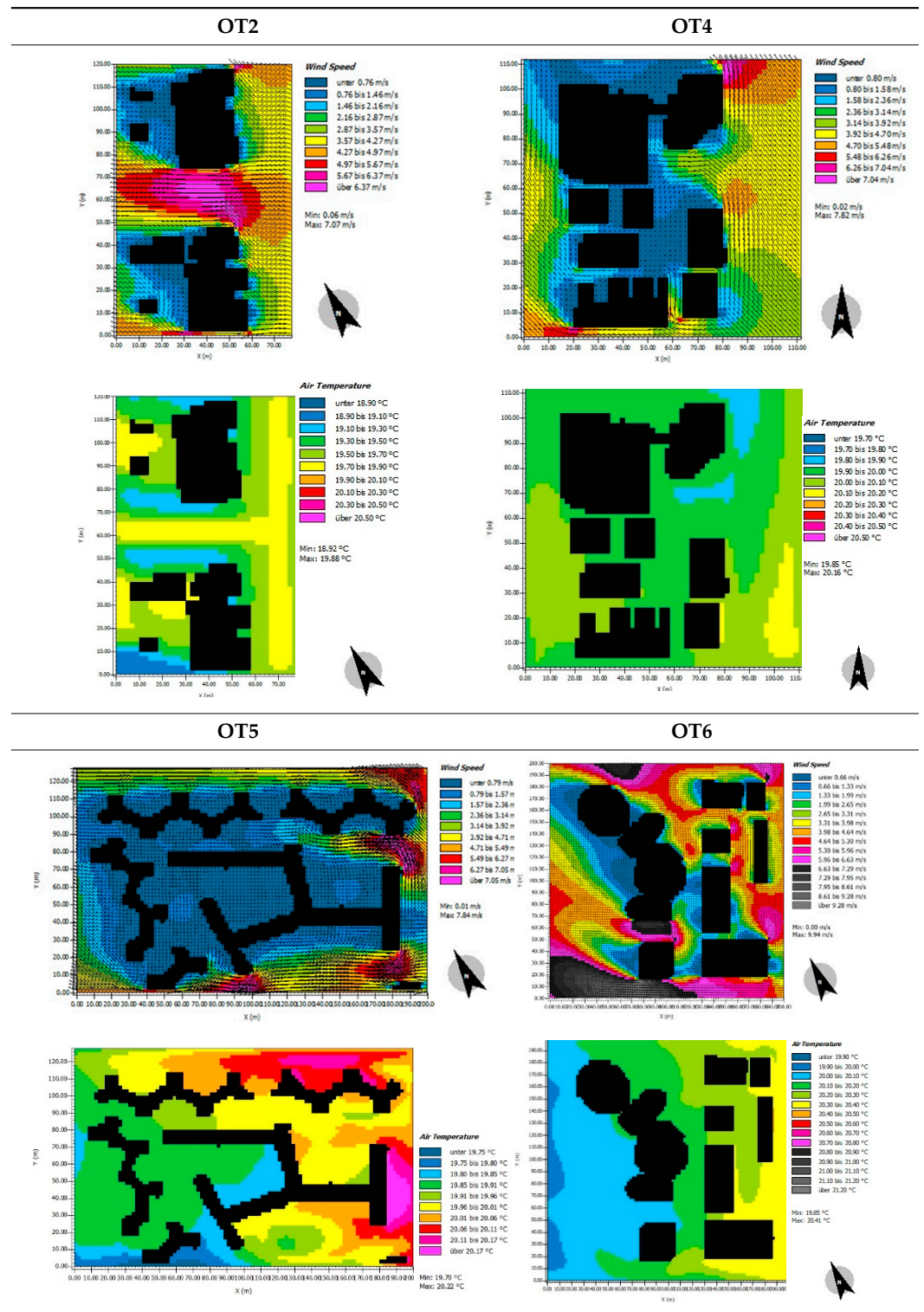
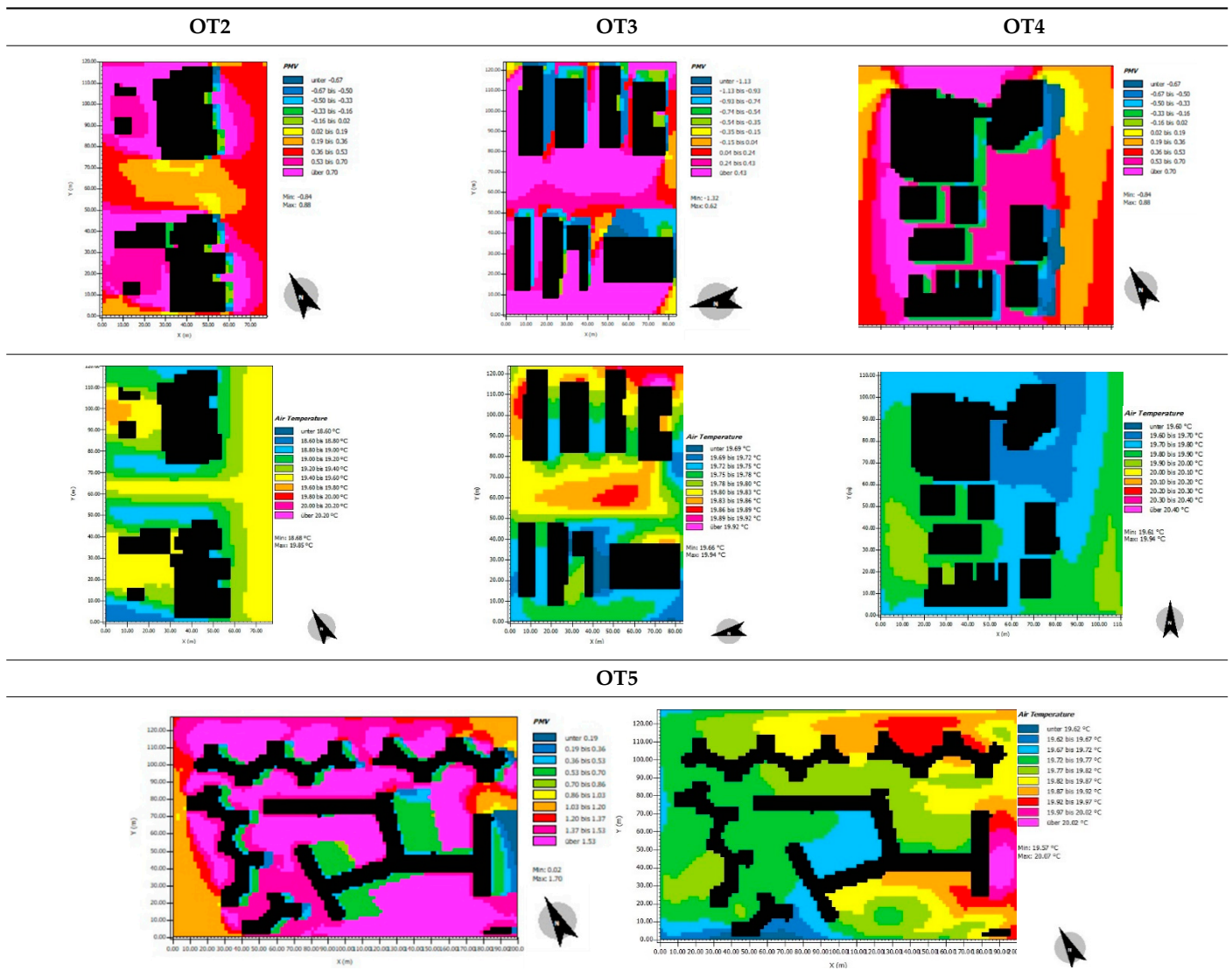


Table 14. Summary of the outdoor thermal comfort based on PMV indices in open-type arrangement on 19 February.



5. Analysis of Results and Discussion

5.1. Layouts Temperature Difference and Wind Speed

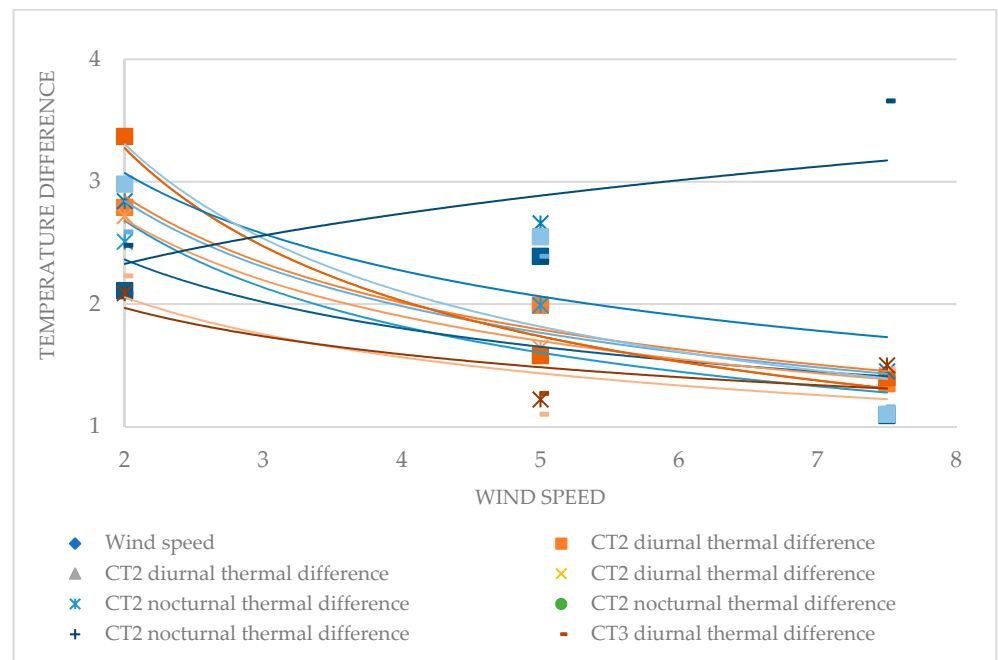
Correlation between the wind speed (horizontal axis), maximum diurnal, and nocturnal (vertical axis) ambient air temperature difference reveals the results for the open and compact arrangements, as presented in Figures 9 and 10, Tables 15 and 16. The diurnal temperature difference ranged from 3.37 °C in CT5 on 17 January with wind speed of 2 m/s to 0.99 °C in CT3 on 19 February with wind speed of 7.5 m/s. Table 15 present a summary of the wind speed and temperature difference in compact arrangements. The overall trend of data shows that the ambient air temperature difference along the layout decline with higher wind speed value in compact-type arrangements. The equation shows that the diurnal temperature difference has a strong correlation with the wind speed value compared to nocturnal as most of the arrangements predicted higher temperature decrease when the wind speed increased. Low-rise arrangements predicted higher temperature decreases than high-rise settlements with higher wind speed values. In connection with low-rise arrangements, the wind flow circulates with a reduced overall material capacity, but in high-rise arrangements, the urban design and building density obstruct the wind flow and trap the heat in their high capacity materials.

Table 15. Wind speed and diurnal (1) and nocturnal (2) temperature difference in compact-type arrangements.

Wind Speed	CT2		CT3		CT4		CT5		CT6		CT7	
	1	2	1	2	1	2	1	2	1	2	1	2
2	2.79	2.51	2.09	2.11	2.72	2.59	3.37	2.84	2.23	2.98	2.09	2.48
5	1.99	1.99	1.27	2.39	1.64	2.39	1.58	2.66	1.1	2.55	1.22	2.35
7.5	1.35	1.1	0.99	1.09	1.42	1.16	1.4	1.45	1.47	1.1	1.5	3.66

Table 16. Wind speed and diurnal (1) and nocturnal (2) temperature difference in open-type arrangements.

Wind Speed	OT2		OT3		OT4		OT5		OT6	
	1	2	1	2	1	2	1	2	1	2
2	3.78	2.13	2.13	2.31	2.72	2.59	2.77	2.86	2.44	2.69
5	2.46	2.32	1.29	2.24	0.92	1.9	1.21	2.79	1.32	3.04
7.5	1.1	1.39	0.93	0.97	1.1	1.44	1.26	1.55	1.1	1.31



Configurations	diurnal regression formula	nocturnal regression formula
CT2	$y = 4.1275x^{-0.519}$	$y = 3.9565x^{-0.561}$
CT3	$y = 3.7107x^{-0.576}$	$y = 3.1005x^{-0.392}$
CT4	$y = 3.8108x^{-0.502}$	$y = 4.073x^{-0.519}$
CT5	$y = 5.2897x^{-0.692}$	$y = 4.1488x^{-0.434}$
CT6	$y = 2.6991x^{-0.393}$	$y = 5.2066x^{-0.655}$
CT7	$y = 2.4369x^{-0.308}$	$y = 1.9793x^{0.2344}$

Figure 9. Correlation between the wind speed on the horizontal axis and maximum diurnal, nocturnal ambient air temperature difference on the vertical axis in Compact Types configurations with their associated regression function formula for diurnal and nocturnal.

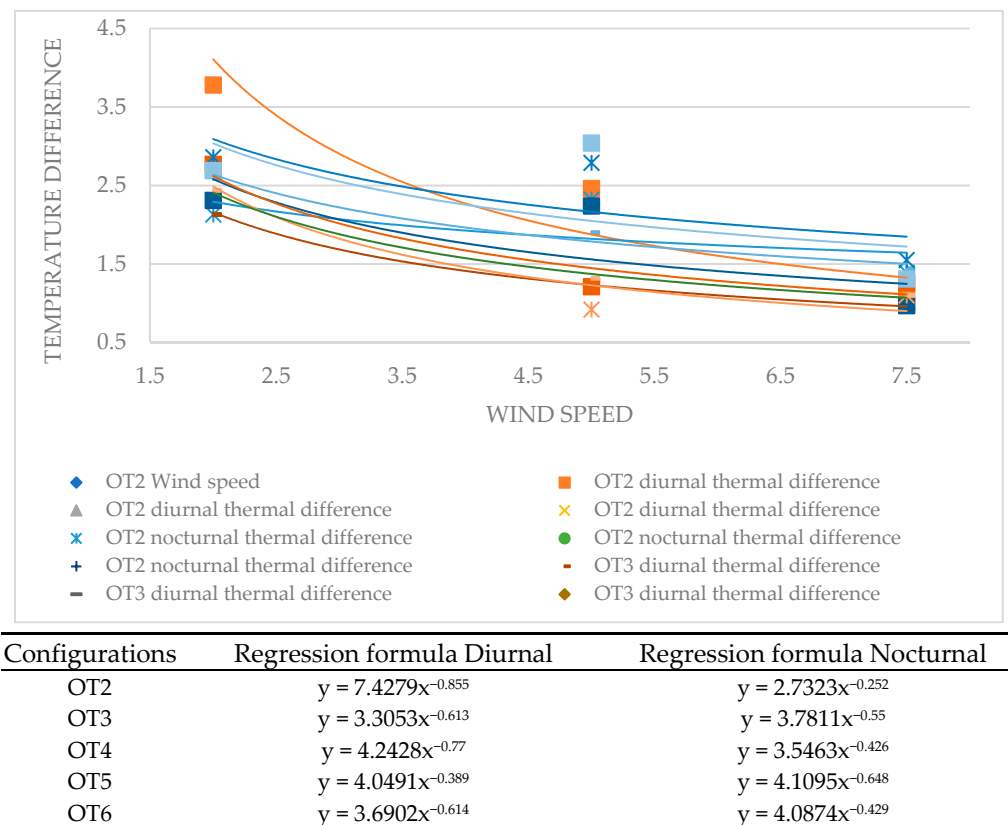


Figure 10. Correlation between the wind speed on the horizontal axis and maximum diurnal, nocturnal ambient air temperature difference on the vertical axis in Open Types configurations with their associated regression function formula.

Analysis of the diurnal/nocturnal regression formula that correlates wind speed and temperature decrease along the compact type arrangements predicted the maximum diurnal temperature decrease along the CT5 arrangement with the equation of $y = 5.2897x^{-0.692}$ and minimum of $y = 2.4369x^{-0.308}$ in CT7 when the wind speed value on these three days. The nocturnal regression formula indicates a decline in temperature decrease in CT7 with the equation of $y = 1.9793x^{0.2344}$ while the CT6 predicted the maximum temperature decrease with the equation of $y = 5.2066x^{-0.655}$.

In open-type arrangements, the diurnal temperature difference ranged from 3.78 °C in OT2 on 17 January to 0.93 °C in OT3 on 19 February. Table 16 present a summary of the wind speed and ambient air temperature difference in open arrangements. Similar results compare to compact type arrangements derived from analysis of the data in Table 15 and Figure 9.

The maximum diurnal temperature decrease along the OT2 arrangement was predicted by analysis of the diurnal/nocturnal regression formula that correlates wind speed and temperature decrease along the open type arrangements to be $y = 7.4279x^{-0.855}$ and the minimum to be $y = 3.6902x^{-0.614}$ in OT6 when the wind velocity value increased on these three days.

Results predicted the maximum diurnal temperature difference of 3.78 °C in OT2 while showing the maximum nocturnal value of 3.66 °C in CT7. The data show a declining trend in the temperature difference when wind speed rises in all configurations. The temperature difference was higher in layouts with an open arrangement than in a compact arrangement. These showed the more advanced cooling potential of the wind in open configurations. Layouts with low-rise settlements and low built up ratio predicted higher intensity in temperature decreases. This is shows the higher built-up ratio in dense urban development highly influence the wind pattern which influence the heat release potential.

Because of the wind-heat advection rate, night-time heat islands have a higher link with wind features. While wind characteristics only influenced diurnal heat islands in low-rise configurations.

5.2. Built-Up Ratio and Average Ambient Temperature

All configurations present the maximum average ambient value on the 17, 24 of January, and 19 of February, respectively. The average temperature ranges from 18.82 °C in OT5 on 19 February to 30.02 in OT4 on 17 January. Figure 11 shows the correlation between the average air temperature at 2 p.m. and the built-up ratio value on three summer days and Table 17 present an average air temperature on 17 (A), 24 January (B), and 19 February (C) at 2 p.m. and built-up ratio in all configurations.

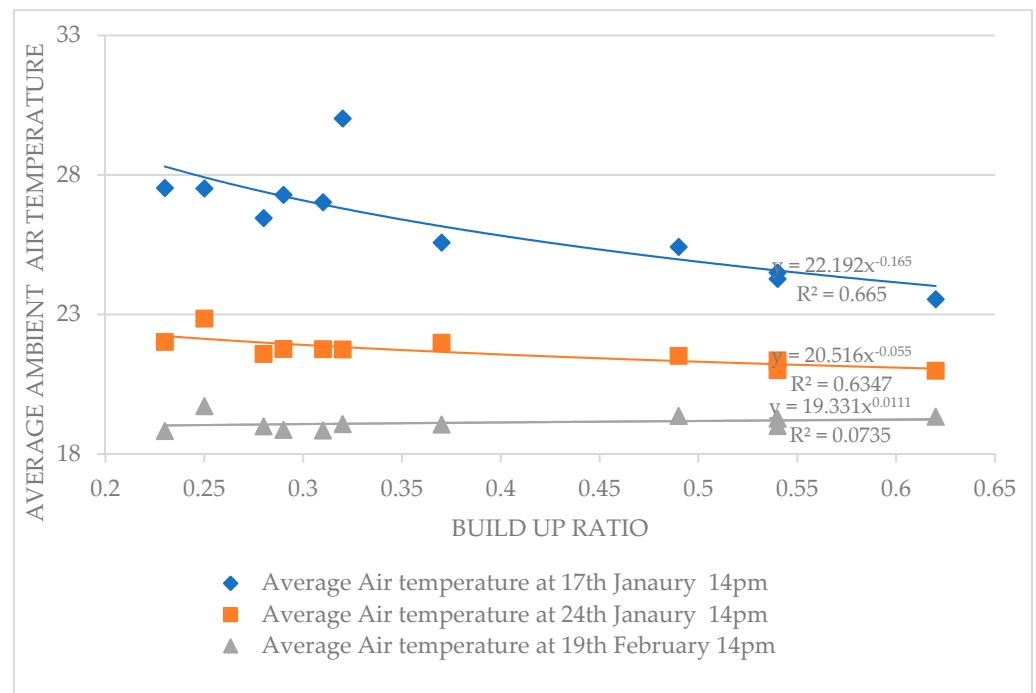


Figure 11. Comparison of the average ambient temperature and built-up ratio on three summer days. 17 January in blue, 24 January in red, 19 February in grey.

Table 17. Average Air temperature on 17 (A), 24 January (B), and 19 February (C) at 2 p.m. and built-up ratio in all configurations.

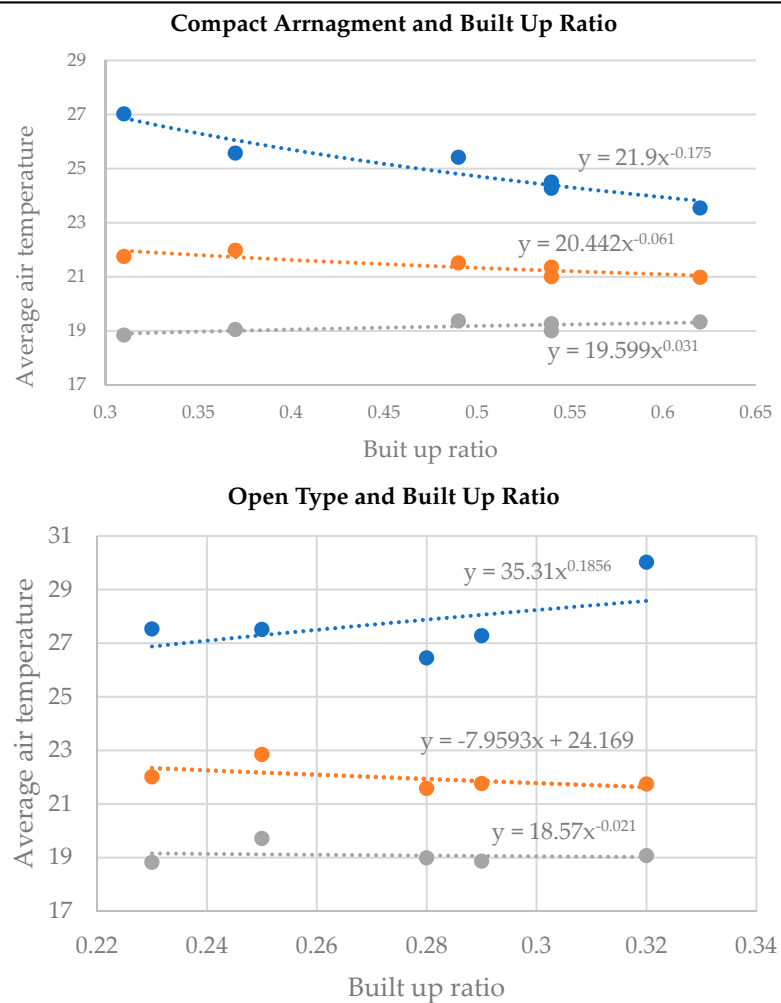
Buildup Ratio	A	B	C	Buildup Ratio	A	B	C	
OT2	0.25	27.51	22.85	CT2	0.49	25.42	21.51	19.36
OT3	0.28	26.45	21.58	CT3	0.31	27.02	21.75	18.84
OT4	0.32	30.02	21.74	CT4	0.54	24.5	21.35	19.26
OT5	0.23	27.53	22.01	CT5	0.62	23.54	20.98	19.33
OT6	0.29	27.28	21.76	CT6	0.37	25.57	21.98	19.05

The interaction between the average air temperature and built-up ratio indicates that on hot summer days with low wind speed (17 January) high built-up ratio arrangements in a high-density urban environment present minimum ambient air temperature. This can be as the result of adjacent building shading effect and low heat advection rate in high built-up ratio urban developments.

On the other hand, on 24 January and 19 February, the urban settlement built-up ratio has slight decrease or no impact on the average ambient air temperature. This can be explained as in moderate to low temperature condition the wind speed impact on the average temperature overweight the built-up ratio effect.

A summary of the comparison between open and compact-type arrangements is presented in Table 18. Open-type arrangements show higher ambient temperature values when the built-up ratio increase on 17 January while presenting a lower value on other two days. On the other hand, compact arrangements predicted lower air temperature with a higher built-up ratio. In addition, there is a higher intensity of temperature decrease in compact arrangements with a higher built-up ratio compared to the open arrangements.

Table 18. A summary of the correlation between average air temperature and built-up ratio in open and compact type arrangements in 17 January dotted in blue, 24 January dotted in orange, 19 February dotted in grey.



Generally, the overall trend of average ambient air temperature shows a constant decrease when the built-up ratio increases in all configurations except the open arrangements on 17 January.

5.3. Built-Up Ratio and Average Wind Speed

The average wind speed value and built-up ratio for three summer days with an initial 2 m/s east, 5 m/s north, and 7.5 m/s south-east wind direction at 2 p.m. were studied and presented in Figure 12. The graph indicates that there is a weak interaction between the built-up ratio and wind speed value in all configurations with a slight decrease in wind speed in high-density arrangements during these three summer days. It could be the result of wind direction alteration and the configurational impact of urban arrangements on wind speed value. Wind shading area increase in the high built-up ratio precincts as the result

of the buildings' wind blockage. However high-rise developments with high aspect ratio canyons still present high wind speed that influence the average calculation. A summary of the mean wind speed value derived from the wind map is presented in Table 19.

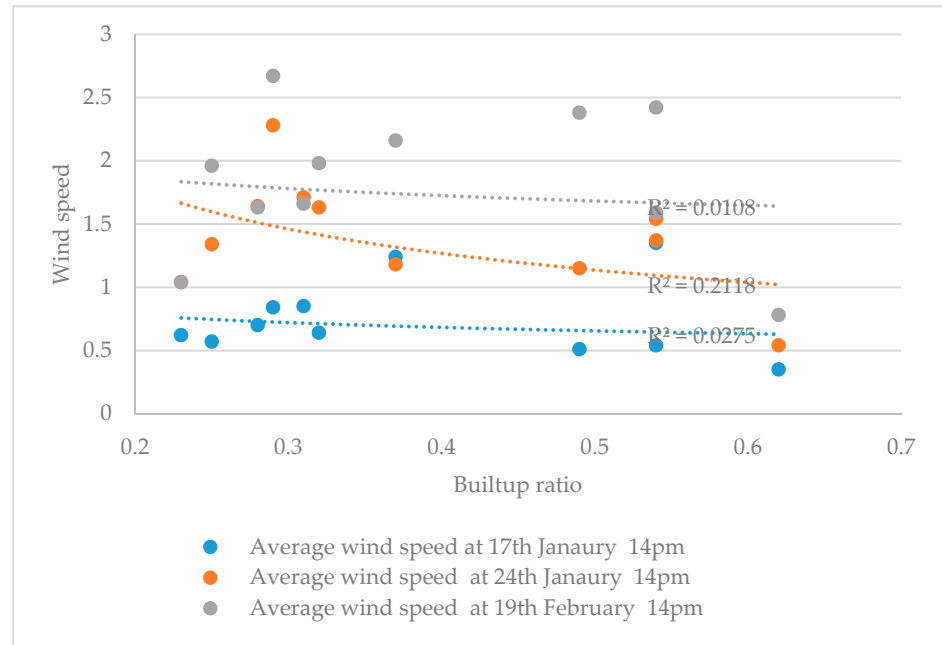


Figure 12. Average wind speed and built-up ratio on 17, 24 January, and 19 February at 2 p.m.

Table 19. Summary of average wind speed value on 17 (A), 24 January (B), 19 February (C) at 2 p.m. and built-up ratio in Compact arrangements.

	Ratio	A	B	C		Ratio	A	B	C
OT2	0.25	0.57	1.34	1.96	CT2	0.49	0.51	1.15	2.38
OT3	0.28	0.7	1.64	1.63	CT3	0.31	0.85	1.71	1.66
OT4	0.32	0.64	1.63	1.98	CT4	0.54	0.54	0.54	1.54
OT5	0.23	0.62	1.04	1.04	CT5	0.62	0.62	0.35	0.54
OT6	0.29	0.84	2.28	2.67	CT7	0.54	1.35	1.37	2.42

The CT5 configuration, with a built-up ratio of 0.62 presents the minimum mean wind speed of 0.35 m/s, while OT6, with a built-up ratio of 0.29, shows the maximum mean wind speed of 2.67 m/s on 17 January. The average wind speed ranges from 0.54 m/s in CT5 to 2.28 m/s in OT6, with a built ratio of 0.29 on 24 January. The average wind speed ranges from 0.78 m/s in CT5 to 2.67 m/s in OT6 on 19 February. The general direction of the data when the built-up ratio increased indicates a constant or slight decrease in the average wind speed value. With the built-up ratio between 0.37 to 0.5, Figure 12 presents a sharp downward trend, and the minimum wind average value shows when the built-up ratio is 0.63 in all three days.

5.4. Built-Up Ratio and Average PMV

Figure 13 and Table 20 illustrates the interaction between average outdoor thermal comfort based on PMV indices and layout built-up ratio at 2 p.m. in all arrangements on three summer days. The graph shows that there is a weak correlation between layout built-up ratio and outdoor thermal comfort on 17 January and 24 January while 19 February shows a strong one. All the arrangements predicted a PMV improvement when the density increased in urban settlements. Urban settlements with a built-up ratio of 0.5 or higher present neutral or cold outdoor conditions on 19 February while on other days all arrangements predicted warm to hot outdoor thermal comfort.

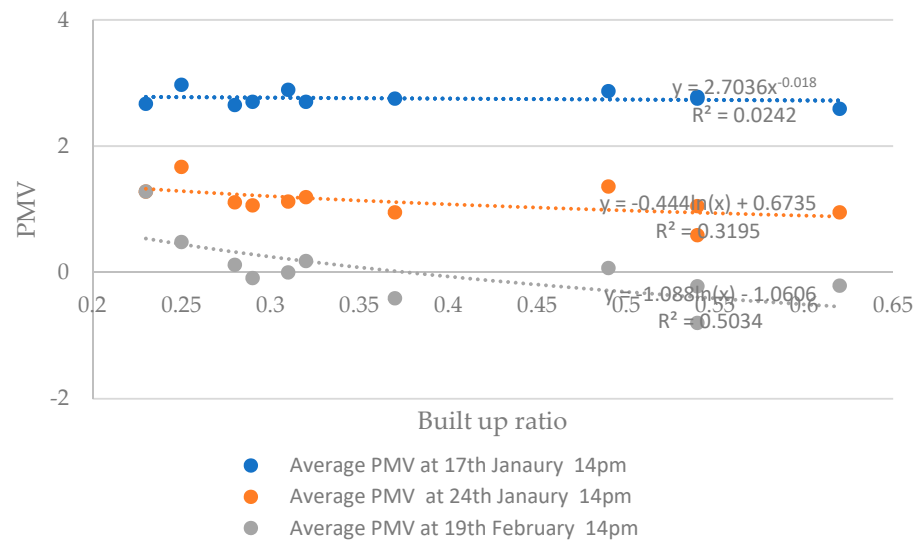


Figure 13. PMV indices and built-up ratio.

Table 20. Summary of PMV indices.

OT Types	Ratio	A	B	C
OT2	0.25	2.97	1.67	0.48
OT3	0.28	2.65	1.11	0.12
OT4	0.32	2.7	1.19	0.18
OT5	0.23	2.67	1.28	1.28
OT6	0.29	2.7	1.06	−0.09
CT Types	Ratio	A	B	C
CT2	0.49	2.87	1.36	0.07
CT7	0.54	2.75	0.59	−0.8
CT4	0.54	2.78	1.05	−0.22
CT5	0.62	2.59	0.95	−0.21
CT6	0.37	2.75	0.95	−0.41

The date of 17 January presents warm to hot outdoor thermal conditions. The average PMV value ranges from 2.59 in CT5 with a layout ratio of 0.62 to 3.58 in OT2 with an area ratio of 0.25. The date of 24 January shows mild to warm conditions and the average PMV ranges from 0.59 in CT7 with a built-up ratio of 0.54 to 1.67 in OT2. The date of 19 February presents slightly cool to slightly warm when the average PMV ranges from −0.80 in CT7 to 1.28 m/s in OT5 with a built ratio of 0.23. Only compact-type configurations on 19 February show minus zero values. The overall trend of the PMV data shows a decrease when the built-up ratio increases in these three days.

5.5. Built-Up Ratio and Average Hourly Temperature Decrease

The average hourly temperature decreases in layout and built-up ratio during the 24-h cycle over three summer days were calculated and presented in Figure 14.

All layouts showed a higher average temperature reduction with a higher built-up ratio.

The general trend of data indicates that configurations with a built-up ratio of 0.25 to 0.37 indicate the higher intensity in temperature decrease while with the built-up ratio of 0.5 or higher, most of the configurations present slight improvement in temperature decrease indices. Analysis of the graphs' equations indicates that the maximum incline presented on 19 February among all three days with a higher temperature decrease intensity. This can be related to the higher wind speed value in these three days.

Furthermore, 17 January presents the maximum temperature decrease records in these three days. The values ranged from 0.55 °C in OT3 on 19 February to 2.13 °C in CT5 on 17 January.

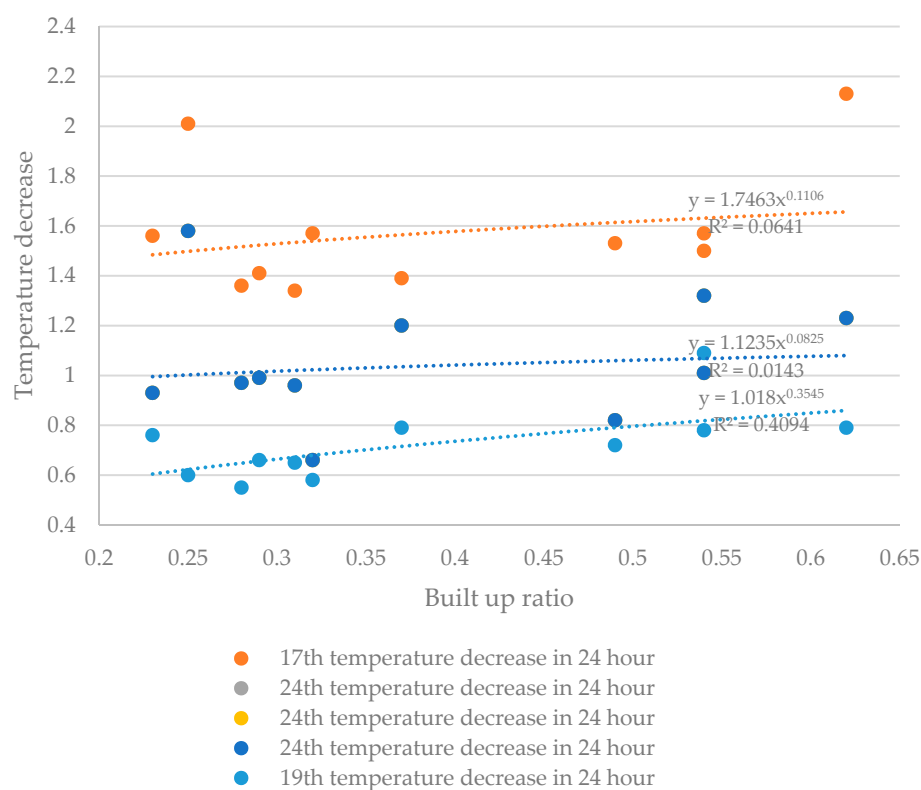


Figure 14. Average hourly temperature decreases in layout and built-up ratio during the 24-h cycle in the three summer days.

6. Conclusions

Sydney's diverse urban fabric suffers from the detrimental effects of overheating, which highly affects the liveability of large portions of the city during heat waves.

These environmental issues deteriorate outdoor health and human well-being. Studying the interaction between urban configurations and heat islands can improve outdoor thermal comfort levels. The results show that:

In terms of outdoor thermal comfort based on PMV indices, increasing of built-up ratio showed a decrease in PMV indices. High built-up ratio layouts predicted more comfortable than low-density layouts on 17 January. The results predicted of similar results for the 19 February with slightly cold in the high built-up ratio to slight warm in low built-up ratio.

Studies of the wind maps indicate that, with an increase in built-up ratio there is a constant or slight decrease in the average wind speed value. With the built-up ratio between 0.37 to 0.5 there is a sharp downward trend in wind velocity, and the minimum of 0.35 when the built-up ratio is 0.63.

In terms of the ambient air temperature, we found that there is a close connection between the built-up ratio and average ambient air temperature, as higher built-up ratio results in lower average ambient temperatures in all settlements. CT5, CT7, CT4, CT2, and CT6 configurations present the minimum average ambient value in their layouts. While OT4, OT2, OT5, OT6, and OT3 predict the maximum average ambient temperature. Studies of the heat maps indicate that a canyon with a north-south orientation in CT5 perpendicular to the wind and an aspect ratio of 4.2 presents the minimum average ambient temperature value. There is a 2.33 °C difference in average temperature values between the maximum (OT4) and the minimum (CT5). These findings highlight the configurational impact of settlement on the heat island effect. In terms of the hourly average temperature decrease, the medium to high-rise compact layouts, including CT5, CT7, CT6, CT4, and CT2, present the maximum average temperature decrease, while OT4, OT3, OT6, and OT5 show the minimum reduction in their layouts, respectively.

Overall, we estimated the environmental advantages of urban configurations on heat island formation under a research method comprising microclimatic modelling and data processing analysis. These findings provide a holistic understanding to urban designers and decision-makers that can be applied in the feasibility study and early design stages. The research findings aid inappropriate urban configurations compatible with Sydney's climate conditions. Finally, we devised a strategy researcher could effectively adopt in other urban sites and tested it in various metropolitan settings and climate conditions.

Author Contributions: Conceptualization, H.R.H.M. and M.S.; methodology, M.S.; software, H.R.H.M.; validation, H.R.H.M.; formal analysis, H.R.H.M.; investigation, H.R.H.M.; resources, M.S.; data curation, M.S.; writing—original draft preparation, H.R.H.M.; writing—review and editing, D.K.; visualization, H.R.H.M.; supervision, L.D.; project administration, H.R.H.M. All authors have read and agreed to the published version of the manuscript.

Funding: This research received no external funding.

Data Availability Statement: Not applicable.

Conflicts of Interest: Authors declare no conflict of interest.

Appendix A

Appendix A.1. Technical Characteristics of the Field Work Measurement Equipment

Table A1. Technical characteristics of the used pyranometers.

Parameter	Value
ISO classification (ISO 9060: 1990)	second class pyranometer
Response time (95 %)	18 s
Zero offset a (response to 200 W/m ² net thermal radiation)	<±15 W/m ² unventilated
Non-linearity	<±1% (100 to 1000 W/m ²)
Directional response	< ± 25 W/m ²
Spectral selectivity	<±5% (0.35 to 1.5 × 10 ⁻⁶ m)
Temperature response	<±3% (−10 to 40 °C)

Table A2. Technical characteristics of the used pyranometers.

Quantity Parameters Value	Quantity Parameters Value	Quantity Parameters Value
Wind	Wind Speed Range	0–60 m/s
	Wind Speed Accuracy	±2% @12 m/s
	Wind Speed Resolution	0.01 m/s
	Wind Direction Range	0 to 359°—No dead band
	Wind Direction Accuracy	±3° @12 m/s
	Wind Direction Resolution	1°
Temperature	Air Temperature	Pt100 1/3 Class B
	Range	−50 °C to +100 °C
	Accuracy	±0.1 °C
	Resolution	0.1 °C
Barometric pressure	Range	600–1100 hPa
	Accuracy	±0.5 hPa

Appendix A.2. Summary of Heat Island Effect in Compact Type Series

Table A3. Summary of heat island effect in compact type series.

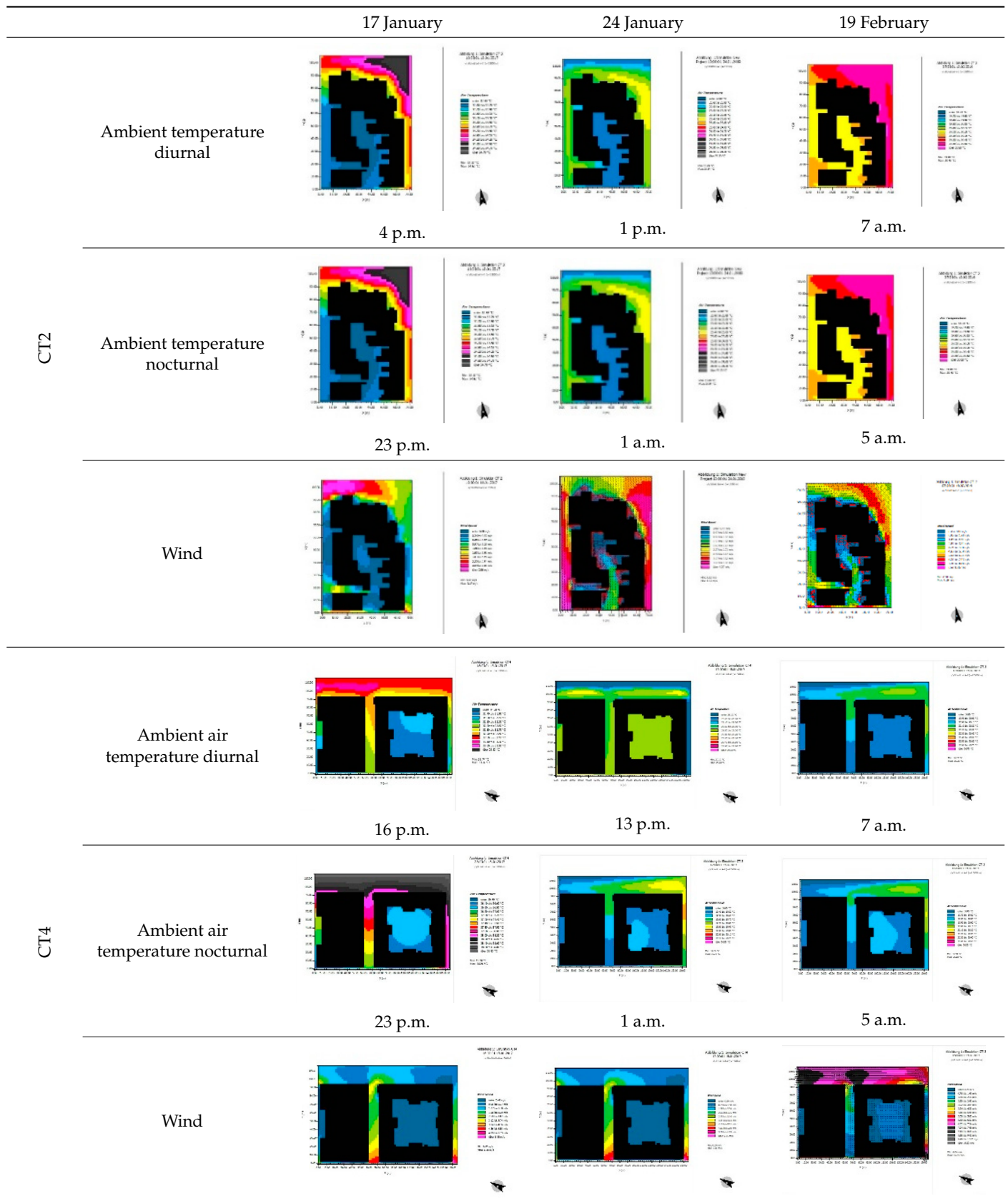
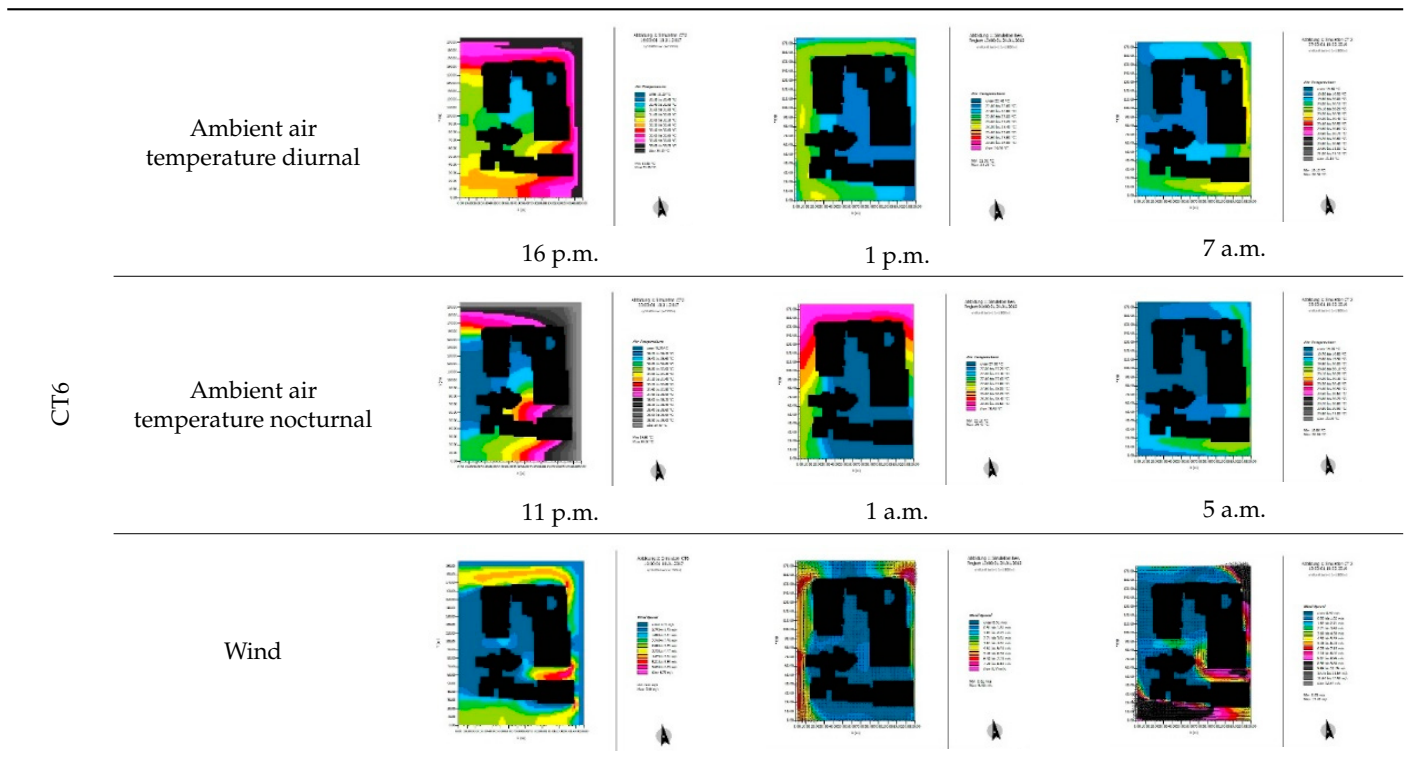


Table A3. Cont.



Appendix A.3. Summary of Heat Island Effect in Open Type Series

Table A4. Summary of heat island effect in open type series.

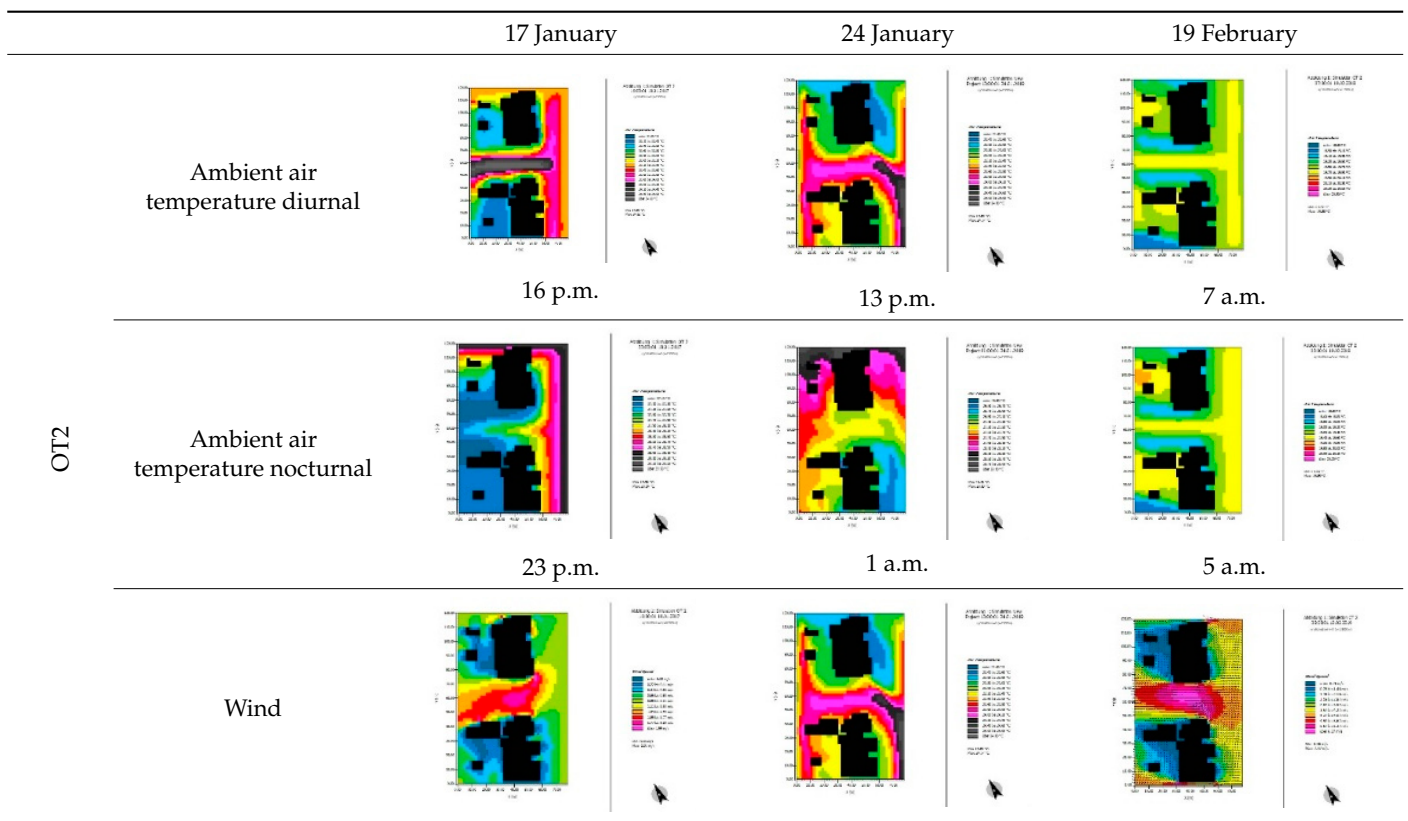
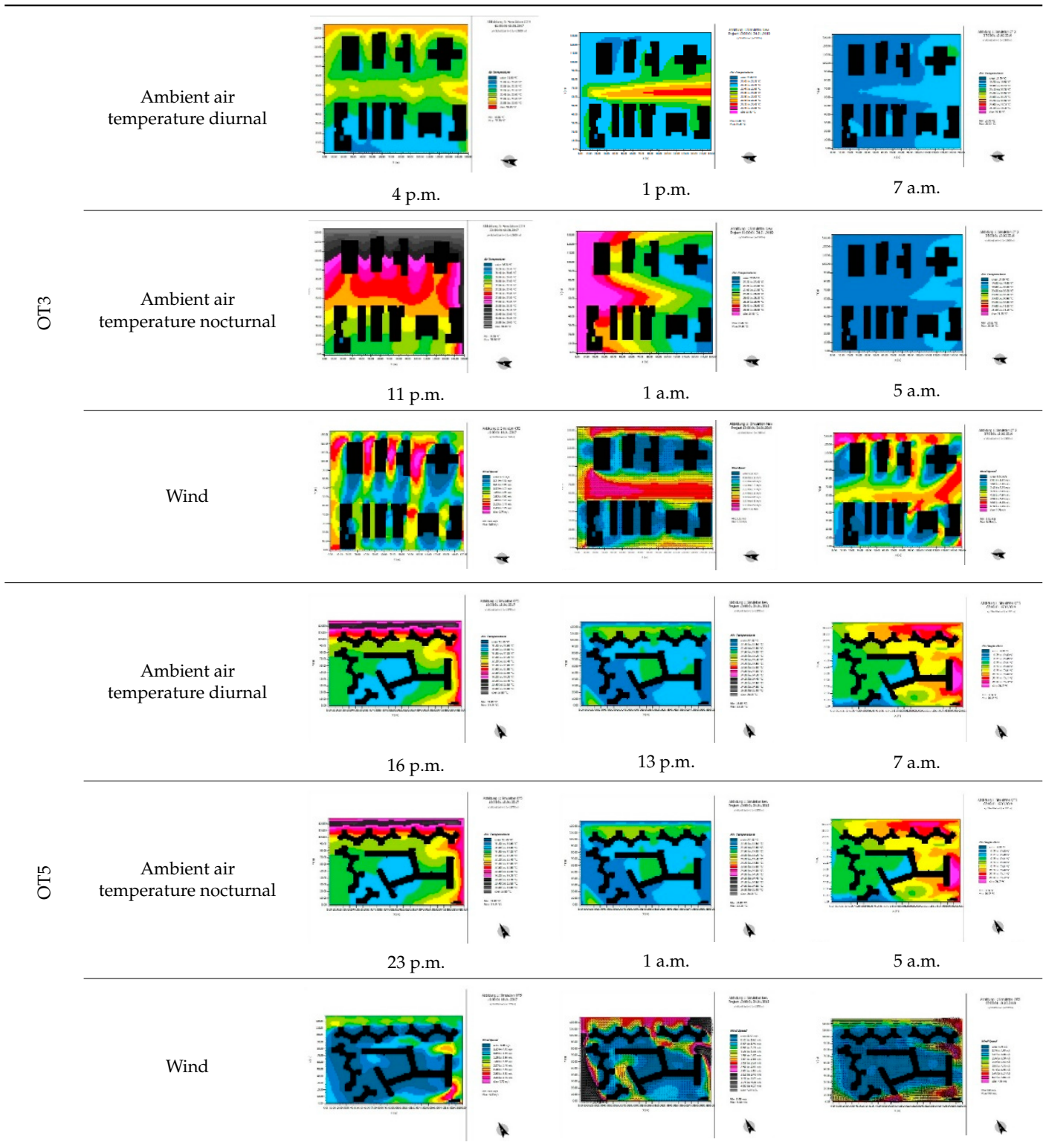


Table A4. Cont.



References

1. Santamouris, M.; Haddad, S.; Saliari, M.; Vasilakopoulou, K.; Synnefa, A.; Paolini, R.; Ulpiani, G.; Garshasbi, S.; Fiorito, F. On the energy impact of urban heat island in Sydney: Climate and energy potential of mitigation technologies. *Energy Build.* **2018**, *166*, 154–164. [[CrossRef](#)]
2. Oke, T.R. *Boundary Layer Climates*; Routledge: London, UK, 2002.
3. Santamouris, M.; Haddad, S.; Fiorito, F.; Osmond, P.; Ding, L.; Prasad, D.; Zhai, X.; Wang, R. Urban Heat Island and Overheating Characteristics in Sydney, Australia. An Analysis of Multiyear Measurements. *Sustainability* **2017**, *9*, 712. [[CrossRef](#)]
4. Oke, T.R. The energetic basis of the urban heat island. *Q. J. R. Meteorol. Soc.* **1982**, *108*, 1–24. [[CrossRef](#)]
5. Khalili, S.M.; Jolai, F.; Torabi, S.A. Integrated production–distribution planning in two-echelon systems: A resilience view. *Int. J. Prod. Res.* **2017**, *55*, 1040–1064. [[CrossRef](#)]
6. Cleugh, H.; Cleugh, H.; Smith, M.S.; Battaglia, M.; Graha, P. *Climate Change: Science and Solutions for Australia*; CSIRO: Canberra, Australia, 2006.
7. Mirmozaffari, M.; Yazdani, R.; Shadk a.m., E.; Khalili, S.M.; Tavassoli, L.S.; Boskabadi, A. A novel hybrid parametric and non-parametric optimisation model for average technical efficiency assessment in public hospitals during and post-COVID-19 pandemic. *Bioengineering* **2021**, *9*, 7. [[CrossRef](#)] [[PubMed](#)]
8. Pearce, K.; Holper, P.; Hopkins, M.; Bouma, W.; Whetton, P.; Hennessy, K.; Power, S. *Climate Change in Australia*; CSIRO: Canberra, Australia, 2007.
9. Wang, X.; Chen, D.; Ren, Z. Assessment of climate change impact on residential building heating and cooling energy requirement in Australia. *Build. Environ.* **2010**, *45*, 1663–1682. [[CrossRef](#)]
10. Rizwan, A.M.; Dennis, L.Y.; Chunho, L. A review on the generation, determination and mitigation of Urban Heat Island. *J. Environ. Sci.* **2008**, *20*, 120–128. [[CrossRef](#)] [[PubMed](#)]
11. Asfour, O. Prediction of wind environment in different grouping patterns of housing blocks. *Energy Build.* **2010**, *42*, 2061–2069. [[CrossRef](#)]
12. Sibevei, A.; Azar, A.; Zandieh, M.; Khalili, S.M.; Yazdani, M. Developing a Risk Reduction Support System for Health System in Iran: A Case Study in Blood Supply Chain Management. *Int. J. Environ. Res. Public Health* **2022**, *19*, 2139. [[CrossRef](#)]
13. Che-Ani, A.; Shahmohamadi, P.; Sairi, A.; Mohd-Nor, M.; Zain, M.; Surat, M. Mitigating the urban heat island effect: Some points without altering existing city planning. *Eur. J. Sci. Res.* **2009**, *35*, 204–216.
14. Santamouris, M.; Papanikolaou, N.; Livada, I.; Koronakis, I.; Georgakis, C.; Argiriou, A.; Assimakopoulos, D. On the impact of urban climate on the energy consumption of buildings. *Sol. Energy* **2001**, *70*, 201–216. [[CrossRef](#)]
15. Steemers, K.; Baker, N.; Crowther, D.; Dubiel, J.; Nikolopoulou, M. Radiation absorption and urban texture. *Build. Res. Inf.* **1998**, *26*, 103–112. [[CrossRef](#)]
16. Morris, C.; Simmonds, I.; Plummer, N. Quantification of the influences of wind and cloud on the nocturnal urban heat island of a large city. *J. Appl. Meteorol. Climatol.* **2001**, *40*, 169–182. [[CrossRef](#)]
17. Shashua-Bar, L.; Tzimir, Y.; Hoffman, M.E. Thermal effects of building geometry and spacing on the urban canopy layer microclimate in a hot-humid climate in summer. *Int. J. Clim.* **2004**, *24*, 1729–1742. [[CrossRef](#)]
18. Thapar, H.; Yannas, S. 491: Microclimate and Urban Form in Dubai. In Proceedings of the 25th Conference on Passive and Low Energy Architecture, Dubai, United Arab Emirates, 22–24 October 2008.
19. Bourbia, F.; Boucheriba, F. Impact of street design on urban microclimate for semi arid climate (Constantine). *Renew. Energy* **2010**, *35*, 343–347. [[CrossRef](#)]
20. Erell, E.; Pearlmutter, D.; Williamson, T. *Urban Microclimate: Designing the Spaces between Buildings*; Routledge: London, UK, 2012.
21. Heshmat Mohajer, H.R.; Ding, L.; Santamouris, M. Developing Heat Mitigation Strategies in the Urban Environment of Sydney, Australia. *Buildings* **2022**, *12*, 903. [[CrossRef](#)]
22. Golany, G.S. Urban design morphology and thermal performance. *Atmos. Environ.* **1996**, *30*, 455–465. [[CrossRef](#)]
23. Yang, Y.; Jin, X.-Y.; Yang, L.-G.; Jin, H.; Xue, M.; Zheng, Z.-Y. Numerical Simulation Research on Pedestrian Wind Environment and Optimization Design of High-Rise Buildings. *Build. Sci.* **2011**, *27*, 4–8.
24. Kolokotsa, D.; Lilli, K.; Gobakis, K.; Mavrigiannaki, A.; Haddad, S.; Garshasbi, S.; Mohajer, H.R.H.; Paolini, R.; Vasilakopoulou, K.; Bartesaghi, C.; et al. Analyzing the Impact of Urban Planning and Building Typologies in Urban Heat Island Mitigation. *Buildings* **2022**, *12*, 537. [[CrossRef](#)]
25. Ali-Toudert, F.; Mayer, H. Numerical study on the effects of aspect ratio and orientation of an urban street canyon on outdoor thermal comfort in hot and dry climate. *Build. Environ.* **2006**, *41*, 94–108. [[CrossRef](#)]
26. Australian Bureau of Statistics. *Australian Statistical Geography Standard (ASGS)*; Australian Bureau of Statistics: Canberra, Australia, 2011.
27. De Dear, R.; Kim, J.; Parkinson, T. Residential adaptive comfort in a humid subtropical climate—Sydney Australia. *Energy Build.* **2018**, *158*, 1296–1305. [[CrossRef](#)]
28. Fahmy, M.; Sharples, S. On the development of an urban passive thermal comfort system in Cairo, Egypt. *Build. Environ.* **2009**, *44*, 1907–1916. [[CrossRef](#)]
29. Krüger, E.L.; Minella, F.O.; Rasia, F. Impact of urban geometry on outdoor thermal comfort and air quality from field measurements in Curitiba, Brazil. *Build. Environ.* **2011**, *46*, 621–634. [[CrossRef](#)]

30. Bruse, M. Modelling and strategies for improved urban climates. In Proceedings of the Proceedings International Conference on Urban Climatology & International Congress of Biometeorology, Sydney, Australia, 8–12 November 1999.
31. Morakinyo, T.E.; Lau, K.K.-L.; Ren, C.; Ng, E. Environment. Performance of Hong Kong's common trees species for outdoor temperature regulation, thermal comfort and energy saving. *Build. Environ.* **2018**, *137*, 157–170. [[CrossRef](#)]
32. Stelling, G.; Zijlema, M. An accurate and efficient finite-difference algorithm for non-hydrostatic free-surface flow with application to wave propagation. *Int. J. Numer. Methods Fluids* **2003**, *43*, 1–23. [[CrossRef](#)]
33. Acero, J.A.; Arrizabalaga, J. Evaluating the performance of ENVI-met model in diurnal cycles for different meteorological conditions. *Arch. Meteorol. Geophys. Bioclimatol. Ser. B* **2016**, *131*, 455–469. [[CrossRef](#)]

Disclaimer/Publisher's Note: The statements, opinions and data contained in all publications are solely those of the individual author(s) and contributor(s) and not of MDPI and/or the editor(s). MDPI and/or the editor(s) disclaim responsibility for any injury to people or property resulting from any ideas, methods, instructions or products referred to in the content.